

## TOPICAL REVIEW

# The Generalized Intersection Approach for Electromagnetic Array Antenna Beam-Shaping Synthesis: A Review

**DANIEL R. PRADO** 

Group of Signal Theory and Communications, Department of Electrical Engineering, Universidad de Oviedo, 33203 Gijón, Spain

e-mail: drprado@uniovi.es


This work was supported in part by the Ministerio de Ciencia, Innovación y Universidades under Project IJC2018-035696-I, in part by the Ministerio de Ciencia e Innovación and the Agencia Estatal de Investigación within Project ENHANCE-5G under Grant PID2020-114172RB-C21/AEI/10.13039/501100011033, and in part by Gobierno del Principado de Asturias under Project AYUD/2021/51706.

**ABSTRACT** This work presents a review of the generalized intersection approach (GIA) for electromagnetic array antenna beam-shaping synthesis. After briefly describing the mechanics of the classical IA, we show the extensions to the IA that make the GIA a more powerful algorithm. In short, these improvements consist in working with the squared field magnitude to improve the convergence properties of the algorithm, and the use of a general minimization algorithm in the backward projection that allows to extend the scope of the optimizing variables beyond those directly related to the field at the aperture. Three optimization examples using the GIA are presented to showcase its capabilities for near and far field synthesis with a variety of arrays: transmitarray, aperiodic phased-array and reflectarray. Finally, we carry out a literature review of the IA, including its origin, different flavours, development, extensions and current and future use for antenna synthesis.

**INDEX TERMS** Generalized intersection approach, alternate projection method, iterative Fourier technique, successive fast Fourier transforms, backward and forward projections, array antenna synthesis.

## I. INTRODUCTION

Electromagnetic array pattern synthesis is an indispensable procedure when non-canonical patterns are required. Examples of applications include transmit antennas for direct broadcast satellite (DBS, also known as direct-to-home or DTH) [1], [2], [3], [4], [5], [6], [7], local multipoint distribution service (LMDS) [8], [9], [10], [11], [12], [13], [14], [15], 5G base stations [16], [17], [18], [19], [20], [21], or crosspolar optimization for various applications such as linear-to-circular reflection polarizers [22], multibeam [23] or DBS [24]. Thus, while classical analytical approaches allow to synthesize collimated beams with certain beamwidth and side-lobe restrictions [25], [26], more modern analytical approaches [27] allow to synthesize shaped-beam patterns,

The associate editor coordinating the review of this manuscript and approving it for publication was Abdullah Iliyasa .

which can then be used as starting point with other more powerful iterative approaches.

However, analytical approaches present limitations when more complex patterns are required, and thus iterative algorithms are employed. The iterative algorithms can be broadly classified into two groups depending on how the search space is navigated. On the one hand, there are the local optimizers, which from one starting initial point, they try to find a solution by applying local changes to the current point. These algorithms usually compute the gradient of a cost function to find the direction in the search space to move to the next candidate solution. In addition, the quality of the solution strongly depends on the starting point of the optimization. Among the iterative local algorithms we find the steepest descend [28], conjugate gradient [29], intersection approach [30], Levenberg-Marquardt (LM) [31] or Broyden-Fletcher-Goldfarb-Shanno (BFGS) [32], among

others. Nevertheless, the steepest descent presents poor converge properties [33], which would make it unsuitable for the synthesis of array antennas with even a moderate number of elements. On the other hand, conjugate gradient methods can be adapted to solve non-linear optimization problems and are faster than the steepest descent [34], but they tend to be both less efficient and less robust than quasi-Newton methods [33], such as the LM and BFGS algorithms. The intersection approach (IA), unlike the previous algorithms, is not based on minimizing a cost function, but rather in finding the intersection between two sets by means of two alternating projections. This is why in the literature it is also known as alternating projection algorithm, or APA. When both projections are implemented by means of the fast Fourier transform (FFT), it is a very fast algorithm. However, as the other local search algorithms, it suffers from the problem of traps or local minima [35].

On the other hand, global search algorithms perform an exhaustive search and do not depend on the starting point. They include genetic algorithms (GA) [36], particle swarm optimization (PSO) [37], ant colony optimization (ACO) [38], bacterial foraging (BF) [39] or simulated annealing [40], among others. A subset of the global search algorithms are known as evolutionary algorithms, since they are based on Darwinian models of biological evolution or animal behaviour. These include GA, PSO, ACO and BF, previously mentioned. Since these algorithms perform an exhaustive search, the starting point is not crucial. In fact, they usually start with a population of random guesses as the starting point. Since the search space grows exponentially with the number of variables, it becomes more difficult to achieve high quality solutions for large arrays with many hundreds or thousands of elements. In order to try to overcome this limitation, some hybrid approaches have been tried, combining local and global search. In any case, some studies have pointed out that the overall performance of the different global search algorithms is very similar for array synthesis [40], [41]. Nevertheless, it seems that for very large arrays with thousands or tens of thousands variables, gradient-based local optimizers are the algorithms of choice [24], [42], [43], [44].

In this work, we present the generalized intersection approach (GIA) for electromagnetic array antenna beam-shaping synthesis. The presented framework is based on that of [35] and particularized for a practical array synthesis with a fixed geometry. We start by introducing the classical implementation of the IA algorithm and some of its limitations in Section II. Solutions to these limitations lead to the redefinition of the forward and backward projections and to the GIA, which is described in Section III. Then, in Section IV we present three examples of application of the GIA for near and far field syntheses involving different types of arrays, namely a transmitarray, an aperiodic phased-array and a reflectarray. Finally, we include a review of the literature on the IA and GIA in Section V, covering its origin,

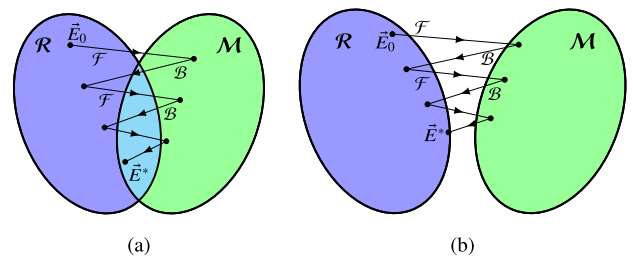


**FIGURE 1. Schematic representation of the intersection approach optimization algorithm. This algorithm is iterative and considers two sets: the set of fields that can be radiated by the antenna ( $\mathcal{R}$ ), and the set of fields that comply with the specifications ( $\mathcal{M}$ ). Starting with an initial guess ( $\vec{E}_0$ ), the algorithm applies two successive operations at each iteration: the forward projection ( $\mathcal{F}$ ) and the backward projection ( $\mathcal{B}$ ) until a solution  $\vec{E}^*$  is reached if the two sets intersect (a), or the minimum distance if the intersection is void (b).**

different flavours, development, extensions and current use for antenna synthesis. Section VI contains the conclusions.

## II. THE CLASSICAL INTERSECTION APPROACH

### A. INTRODUCTION

The intersection approach (IA) is a local search iterative algorithm that, in its classical implementation [30], works with two sets: the set of electromagnetic fields that can be radiated by the antenna (set  $\mathcal{R}$ ), and the set of electromagnetic fields that comply with the requirements (set  $\mathcal{M}$ ). At each iteration  $n$ , the IA performs the following operations:

$$\vec{E}_{n+1} = \mathcal{B} \left\{ \mathcal{F} \left\{ \vec{E}_n \right\} \right\}, \quad (1)$$

where  $\vec{E}_n$  is the field radiated by the antenna at iteration  $n$  of the algorithm,  $\mathcal{F}$  is known as the forward projection and  $\mathcal{B}$  is the backward projection. The forward projection projects field  $\vec{E}$  onto the set of radiated fields that comply with the specifications, but in general cannot be radiated by the antenna. Meanwhile, the backward projection projects the radiated field which fulfils specifications onto the set of fields that can be radiated by the antenna. The aim of the sequence defined in (1) is to find the intersection between the two sets, or if that is not possible because the intersection is void, to find a radiated field belonging to set  $\mathcal{R}$  whose distance to the set  $\mathcal{M}$  is minimal. FIGURE 1 shows a schematic representation of this procedure. In addition, with this definition the IA may be applied to both near and far field synthesis problems.

The definition of the  $\mathcal{F}$  and  $\mathcal{B}$  projections will vary depending on the type of antenna, constraints applied, etc. [35]. For the particular case of planar electromagnetic array antennas considered in this work, one of the advantages of defining the iteration of the IA as in (1) is that both projections may use the FFT algorithm to calculate the radiated field from the field at the aperture ( $\mathcal{F}$  projection), and to recover the field at the aperture from the radiated field ( $\mathcal{B}$  projection). This results in a computationally extremely efficient algorithm, since the most expensive operation would be the FFT.

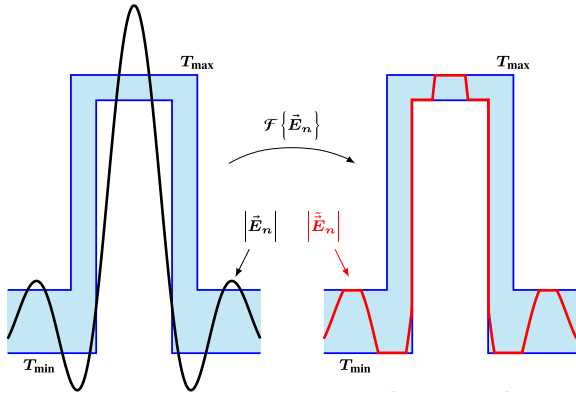


**FIGURE 2.** Schematic illustration of the operation performed by the forward projection in the classical intersection approach: given an element of set  $\mathcal{R}$ , (in this case the field magnitude radiated by the antenna, in black), it projects the field onto set  $\mathcal{M}$ , obtaining a “trimmed” field magnitude (in red) that complies with the specifications ( $T_{\min}$  and  $T_{\max}$ ) but that in general cannot be radiated by the antenna.

Before describing both projections, it is worth mentioning that the radiated field depends on several parameters, including the observation point, optimizing variables, etc. However, in order to alleviate the notation in the algorithm equations in Sections II and III, the dependencies on these variables are dropped. Concrete dependence on these variables may be found in Section IV when applied to specific types of arrays.

### B. THE FORWARD PROJECTION

Given an upper bound template denoted as  $T_{\max}$ , and a lower bound template denoted as  $T_{\min}$ , both given in the far field, the forward projection at iteration  $n$  is given by [30]:

$$\tilde{\tilde{E}}_n = \mathcal{F}\{\tilde{E}_n\} = \begin{cases} T_{\max} \frac{\tilde{E}_n}{|\tilde{E}_n|}, & |\tilde{E}_n| > T_{\max} \\ T_{\min} \frac{\tilde{E}_n}{|\tilde{E}_n|}, & |\tilde{E}_n| < T_{\min} \\ \tilde{E}_n, & \text{otherwise.} \end{cases} \quad (2)$$

A schematic representation of this operation is shown in FIGURE 2. This projection ensures that the field  $\tilde{\tilde{E}}_n$  complies with the imposed specifications, that is, that it belongs to set  $\mathcal{M}$  by complying:

$$T_{\min} \leq |\tilde{\tilde{E}}_n| \leq T_{\max}. \quad (3)$$

However, field  $\tilde{\tilde{E}}_n$  does not in general belong to set  $\mathcal{R}$ , i.e., it cannot be radiated by the antenna.

### C. THE BACKWARD PROJECTION

The backward projection is a multi-step operator. First, the field at the aperture of the array is calculated. Since we are dealing with planar arrays, the Fourier transform may be applied in the form of the fast Fourier transform (FFT):

$$\tilde{E}_{\text{ap},n} = C_1 \text{FFT}\{C_2 \tilde{\tilde{E}}_n\}, \quad (4)$$

where  $\tilde{E}_{\text{ap},n} = \{E_{\text{ap},n}^i\}$ ,  $i = 1, \dots, I$  is the field at the aperture of an array comprised of  $I$  elements indexed by  $i$  at iteration  $n$  of the algorithm, and  $C_1$  and  $C_2$  are some constants that depend on the type of planar array being synthesized [30], [45].

Second, the backward projection applies some restrictions on the field at the aperture. For instance, in array synthesis one may desired to limit the dynamic range of the amplitude or impose certain phase restrictions [30]. A limit to the dynamic range of the amplitude between values  $E_{\text{ap},\min}$  and  $E_{\text{ap},\max}$  is imposed as:

$$\tilde{E}_{\text{ap},n}^i = \begin{cases} E_{\text{ap},\max} \frac{E_{\text{ap},n}^i}{|E_{\text{ap},n}^i|}, & |E_{\text{ap},n}^i| > E_{\text{ap},\max} \\ E_{\text{ap},\min} \frac{E_{\text{ap},n}^i}{|E_{\text{ap},n}^i|}, & |E_{\text{ap},n}^i| < E_{\text{ap},\min} \\ E_{\text{ap},n}^i, & \text{otherwise,} \end{cases} \quad (5)$$

for each array element  $i = 1, \dots, I$ . Meanwhile, a limit to the phase variation of the field at the aperture may be achieved with:

$$\angle \tilde{E}_{\text{ap},n}^i = \begin{cases} \angle E_{\text{ap},n}^i, & \forall i / \Delta\phi_{n,i} \leq \Delta\phi_{\max}, \\ \angle E_{\text{ap},n}^0, & \forall i / \Delta\phi_{n,i} > \Delta\phi_{\max}, \end{cases} \quad (6)$$

where

$$\Delta\phi_{n,i} = \left| \angle E_{\text{ap},n}^i - \angle E_{\text{ap},0}^i \right|, \quad (7)$$

$\angle E_{\text{ap},n}^i$  is the phase of the field at the aperture for iteration  $n$  and array element  $i = 1, \dots, I$  (when  $n = 0$  it corresponds to the initial field at the aperture), and  $\Delta\phi_{\max}$  is the maximum allowable variation in the phase. In the case of phased arrays, reflectarrays or transmitarrays that present a fixed magnitude of the field at the aperture, this magnitude must be preserved throughout the synthesis process by imposing the following constraint:

$$\tilde{E}_{\text{ap},n}^i = |E_{\text{ap},0}^i| \exp\{j\angle E_{\text{ap},n}^i\}, \quad (8)$$

for  $i = 1, \dots, I$ .

After the field at the aperture has been obtained and restrictions to it have been applied as needed, the far field is calculated again using the inverse FFT:

$$\tilde{E}_{n+1} = C_3 \text{IFFT}\{C_4 \tilde{E}_{\text{ap},n}\}, \quad (9)$$

where  $C_3$  and  $C_4$  are some constants that depend on the type of planar array being synthesized [30], [45].

Once the field  $\tilde{E}_{n+1}$  has been obtained, it is checked whether it complies with the specifications. If it complies, the algorithm finishes. If it does not comply, a new iteration will be carried out applying the same process, first with the forward projection and the with then backward projection. Finally, although this process has been illustrated for the far field, the same procedure may be applied to the near field by substituting (4) and (9) by the appropriate near field

equations [46], since the application of the forward projection and constraints on the field at the aperture remain the same.

#### D. DRAWBACKS OF THE CLASSICAL IA

However, the implementation of the IA following (1) with the FFT in both projections presents two main drawbacks. The first issue is related to the use of the FFT to implement the backward projection. The FFT allows to recover the field at the aperture from the radiated field (either near field by using the representation in terms of its plane wave spectrum [47], or far field since it is essentially the Fourier transform of the field at the aperture [48]). This means that only variables directly related to the tangential field at the aperture may be optimized, i.e., the complex excitation for arrays (magnitude and/or phase), or only the phase-shift (for instance in phased-arrays, reflectarrays and transmitarrays), which limits the applicability of the synthesis procedure to copolar patterns and monochromatic cases, since the complete electromagnetic response of the array element may not be easily included in the synthesis loop.

On the other hand, the second drawback is the fact that the IA presents the so-called problem of traps or local minima [30]. They arise due to two reasons: the number of degrees of freedom (DoF) available and the non-convexity of the sets  $\mathcal{R}$  and  $\mathcal{M}$ . Here we define the DoF as the optimizing variables in the synthesis procedure. This problem can be alleviated by addressing both sources of local minima. Firstly, the initial number of DoF can be small and then be progressively increased in successive stages until all of them are considered in the synthesis. This reduces the number of local minima in the first stages to facilitate convergence of the algorithm towards a solution. And secondly, if instead of choosing the radiated field  $\vec{E}$  as in (1) we employ the squared magnitude of the field, i.e.  $|\vec{E}|^2$  (or equivalently the gain  $G$  in far field applications, since  $G \propto |\vec{E}|^2$ ), it turns  $\mathcal{R}$  into a convex set [35], which minimizes the number of local minima in the synthesis process. (Please note that set  $\mathcal{M}$  is still non-convex [35].)

Addressing these two main drawbacks leads to the GIA, which will be described next.

### III. THE GENERALIZED INTERSECTION APPROACH

#### A. EXTENDING THE CLASSICAL IA

The GIA redefines sets  $\mathcal{M}$  and  $\mathcal{R}$  to employ the squared magnitude of the radiated field. In such a case, the GIA performs the following operation:

$$|\vec{E}_{n+1}|^2 = \mathcal{B} \left\{ |\vec{E}_n|^2, \mathcal{F} \left\{ |\vec{E}_n|^2 \right\} \right\}, \quad (10)$$

which is similar to the one in (1), but with the squared field magnitude. As explained earlier, using the squared field magnitude,  $\mathcal{R}$  turns into a convex set [35], thus reducing the number of local minima and improving convergence [49], [50]. However, it has another consequence in the definition of the backward projection. Since now the squared field magnitude is employed, the tangential field at the aperture may not be

recovered by employing the FFT [24]. In this case, a general minimization algorithm must be employed in the backward projection as it will be later described. This in turn allows to generalize the scope of the optimizing variables, since now we are not restricted to only work with the tangential field recovered by the FFT, as it was the case of the IA.

In general, we can consider a set of optimizing variables  $\vec{x}_{k,n} = \{x_{k,n} \in \mathcal{X} \subseteq \mathbb{R}; k = 1, \dots, K\}$ , which are related to the radiated field through the propagation operator:

$$|\vec{E}_n|^2 = \mathcal{P} \{ \vec{x}_{k,n} \}. \quad (11)$$

In general, the number of optimizing variables  $K$  can be different from the number of array elements  $I$  since only a subset of the elements may be optimized, each element may have more than one variable, or a combination of the two. Since this algorithm may be applied to different kinds of arrays, the optimizing variables can differ in nature. For instance, it may be the tangential field for classic arrays, i.e., the magnitude and phase of its excitations [30]; or only the phases in the case of phased-arrays [31]. In the case of reflectarray antennas, it would be the reflection phase [51]; the transmission phase for transmitarrays or lenses [52]; or the surface impedance for metasurfaces [53]. Geometrical features of the unit cell can also be the optimizing variables for a direct layout optimization [24]. In contrast, the optimizing variables of the classical IA were the ones directly related to the tangential field at the aperture, that is, its magnitude and/or phase. Thus, the GIA generalizes the scope of the optimizing variables, allowing for instance the direct layout optimization of arrays that is not possible with the classical IA. An example of this will be shown in Section IV.

The operator  $\mathcal{P}\{\cdot\}$  thus involves any operation that translates the optimizing variables into the radiated field, and will depend on the nature of those variables. For instance, if  $\vec{x}_{k,n}$  is the complex excitation of an array,  $\mathcal{P}\{\cdot\}$  would involve computing the array factor. Or if a direct layout optimization is performed, for instance of a reflectarray antenna as in [24], a full-wave analysis tool based on local periodicity is employed to obtain the reflected tangential field, from which the radiated field is then obtained. Since the concrete formulation of  $\mathcal{P}\{\cdot\}$  depends on the type of antenna that is being synthesized and the considered radiated field (either near or far field), particular expressions are provided in Section IV for three different types of planar arrays.

FIGURE 3 shows a schematic representation of the process followed by the GIA, where the backward projection is performed by the Levenberg-Marquardt (LM) algorithm, although any other minimizing algorithm could have been chosen [24]. In a generic iteration  $n$ , the GIA computes an element of  $\mathcal{R}$  by applying (11). Then, it applies the forward projection  $\mathcal{F}$ . The backward projection  $\mathcal{B}$  is represented by a dashed line since it does not go directly from  $\mathcal{M}$  to  $\mathcal{R}$ , but instead, and using a minimization algorithm (the LM in this case), searches for a new set  $\vec{x}_{k,n+1}$  such that  $\mathcal{P} \{ \vec{x}_{k,n+1} \}$  is closer to the  $\mathcal{M}$  set than  $\mathcal{P} \{ \vec{x}_{k,n} \}$ . This is represented, for

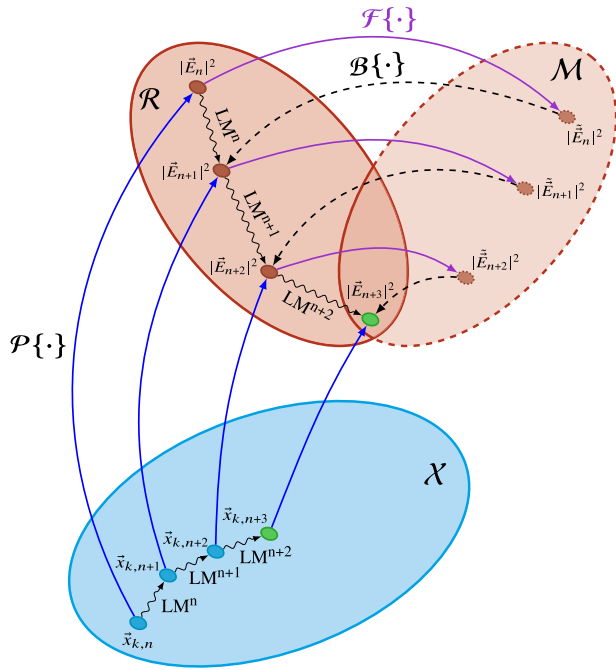


**FIGURE 3.** Schematic representation of the generalized intersection approach (GIA) optimization algorithm. Similarly to the classical IA, the GIA considers the same two sets  $\mathcal{R}$  and  $\mathcal{M}$ , and applies iteratively the forward ( $\mathcal{F}$ ) and backward ( $\mathcal{B}$ ) projections until a solution is reached. However, there are two main differences: it considers the square magnitude of the radiated field,  $|\vec{E}|^2$ ; and now the backward projection is implemented by means of a general minimization algorithm, here illustrated by the use of the Levenberg-Marquardt (LM) algorithm. The  $\mathcal{P}\{\cdot\}$  operator relates the optimizing variables (belonging to set  $\mathcal{X}$ ) in the array aperture with the radiated field.

iteration  $n$  by the wavy line denoted with  $\text{LM}^n$  in both the  $\mathcal{X}$  and  $\mathcal{R}$  sets.

It is also worth mentioning that the GIA is a local optimizer, and thus the starting point for the optimization is of great importance, since it will determine the quality of the obtained results. In this regard, the closer the starting point is to the solution, the better. In [30] it is recommended, for shaped and contour beam arrays to start with an analytical phase-only synthesis (POS), and then refine that result with the application of the (G)IA algorithm. This approach was used, for instance, in [11], where the analytical POS described in [27] was used to obtain a suitable starting point for the IA synthesis. However, it has been shown that starting with a properly focused beam is a good enough starting point for a general optimization procedure [54]. In addition, the convergence properties and computational efficiency of the algorithm mainly depend, to a great extent, on the definition of both projections.

In the following, we will briefly review the basic and generic definitions of the forward and backward projections as applied in the GIA algorithm.

### B. THE FORWARD PROJECTION IN THE GIA

In the GIA, the forward projector is similar to that described in (2), but applied to the squared field magnitude. Thus, the

maximum and minimum templates employed in the IA,  $T_{\min}$  and  $T_{\max}$ , must be squared to be expressed in the same units of the squared field magnitude. Then, the forward projection at iteration  $n$  is given by:

$$|\tilde{\vec{E}}_n|^2 = \mathcal{F} \left\{ |\vec{E}_n|^2 \right\} = \begin{cases} T_{\max}^2, & |\vec{E}_n|^2 > T_{\max}^2 \\ T_{\min}^2, & |\vec{E}_n|^2 < T_{\min}^2 \\ |\vec{E}_n|^2, & \text{otherwise.} \end{cases} \quad (12)$$

The schematic representation shown in FIGURE 2 serves to illustrate (12) as well, but changing the field magnitude with the squared field magnitude.

Although the operation in (12) is the basic definition of forward projection, it is by no means the only possible. Indeed, the operation in (12) only imposes restrictions on an element of set  $\mathcal{R}$ . However,  $\mathcal{F}$  can involve more operations if a more complex algorithm is desired. For example, in [24] two forward projections are defined depending on whether the synthesis is carried out in float gain ( $T_{\min}^2$  and  $T_{\max}^2$  are adjusted depending on the value of  $|\vec{E}_n|^2$  in the current iteration) or in fixed gain ( $T_{\min}^2$  and  $T_{\max}^2$  have a fixed value regardless of  $|\vec{E}_n|^2$ ). Other possibilities are reviewed in Section V.

Please note that despite being only concerned with the squared field magnitude  $|\vec{E}_n|^2$ , some applications also require the optimization of the radiated field phase in addition to the magnitude. A relevant case would be that of plane wave generators, in which a quiet zone is generated in front of the antenna whose near field magnitude and phase need to comply with certain restrictions, typically 1 dB of ripple in magnitude and  $10^\circ$  of ripple in phase. In such a case, the GIA may be extended to include both squared field magnitude and field phase constraints as in [55]. The application of (12) for the field phase would be equivalent, provided appropriate values of the minimum and maximum templates.

### C. THE BACKWARD PROJECTION IN THE GIA

In the GIA, the backward projection consists in decreasing the distance between the new element  $|\tilde{\vec{E}}_n|^2 = \mathcal{F}\{|\vec{E}_n|^2\}$  and set  $\mathcal{R}$ . This is represented by the  $\mathcal{B}\{\cdot\}$  operator in FIGURE 3. This is achieved by considering the current radiated field by the antenna at iteration  $n$ ,  $\vec{E}_n$ , and decreasing the distance with its forward projection:

$$\begin{aligned} |\tilde{\vec{E}}_{n+1}|^2 &= \mathcal{B} \left\{ |\vec{E}_n|^2, |\tilde{\vec{E}}_n|^2 \right\} \\ &= \text{decrease dist} \left( |\vec{E}_n|^2, |\tilde{\vec{E}}_n|^2 \right). \end{aligned} \quad (13)$$

As a definition of distance in (13), the Euclidean norm for square-integrable functions can be used, which may be easily implemented by a weighted Euclidean metric [24]:

$$d = \text{dist}^2 \left( |\vec{E}_n|^2, |\tilde{\vec{E}}_n|^2 \right) = \int_{\Omega} w_{\Omega} \left( |\vec{E}_n|_{\Omega}^2 - |\tilde{\vec{E}}_n|_{\Omega}^2 \right)^2 d\Omega, \quad (14)$$

where  $\Omega$  is the region where the radiated field is calculated and  $w_\Omega$  is a weighting function. For the computation of the field, the region  $\Omega$  is discretized into a number of points  $L$ . Then, the integral in (14) can be expressed as:

$$d = \sum_{l=1}^L w_l \left( \left| \vec{E}_n \right|_l^2 - \left| \tilde{\vec{E}}_n \right|_l^2 \right)^2 \Delta\Omega, \quad (15)$$

where index  $l$  indicates each of the points where the radiated field is discretized, and  $\Delta\Omega$  is the step of the discretization.

The expression of the distance in (15) can be easily minimized by a general optimization algorithm. For instance, in [35] a descent method is suggested, in [56] the BFGS algorithm is used, the Fletcher-Powell (FP) algorithm is employed in [57], and the LM is employed in [24]. In addition, it is important to notice that it is not necessary to attain the minimum of (13)–(15), only to decrease the distance [35]. Thus, just a few iterations of the minimization algorithm are required in the backward projection. For instance, in [24] and [57] three iterations of the LM and FP, respectively, are employed each time the backward projection is applied.

This step is represented by the wavy lines in FIGURE 3, in both the  $\mathcal{R}$  and  $\mathcal{X}$  sets. To decrease (15), the starting iteration of the minimization algorithms considers the current solution at iteration  $n$  of the GIA, i.e., the vector of current optimizing variables  $\vec{x}_{k,n}$  and the current squared radiated field magnitude  $|\vec{E}_n|^2 = \mathcal{P}\{\vec{x}_{k,n}\}$ . The “trimmed” field  $|\tilde{\vec{E}}_n|^2 = \mathcal{F}\{|\vec{E}_n|^2\}$  is considered the reference for this minimization. As the minimization algorithm iterates, it transverse the  $\mathcal{X}$  set of optimizing variables searching for a radiated field in the  $\mathcal{R}$  set that is closer to  $\mathcal{F}\{|\vec{E}_n|^2\}$ .

As it was the case of the classical IA, sometimes it is necessary to impose certain constraints on the optimizing variables. The restrictions of (5)–(8) may be also applied to the GIA by simply identifying  $\vec{x}_{k,n}$  with some values of  $\vec{E}_{ap,n}^i$ ,  $|\vec{E}_{ap,n}^i|$  or  $\angle \vec{E}_{ap,n}^i$ , depending on whether the optimizing variables are the complex excitation of the planar array (i.e., the field at the aperture), its magnitude, or its phase, respectively. Moreover, as mentioned before the GIA allows to extend the scope of the optimizing variables beyond those directly related to the field at the aperture. A common example is direct layout optimizations [24], [42], where the geometrical features of a unit cell are the optimizing variables, such as the dimensions of a rectangular patch [58] or the length of dipoles [24]. For the application of this constraint we assume that the minimum and maximum allowed dimensions are  $x_{\min}$  and  $x_{\max}$ , respectively. Then, the optimizing variables would be constrained by:

$$\tilde{\vec{x}}_{k,n} = \begin{cases} x_{\max}, & \forall k / \vec{x}_{k,n} > x_{\max} \\ x_{\min}, & \forall k / \vec{x}_{k,n} < x_{\min} \\ \vec{x}_{k,n}, & \text{otherwise.} \end{cases} \quad (16)$$

Other restrictions might also apply, for instance if orthogonal dipoles are used such that they do not overlap with each other in dual polarized unit cells [24], [59].

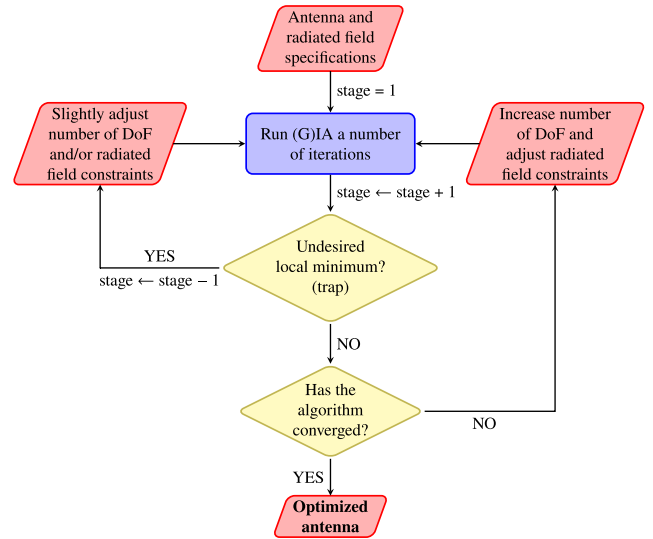


FIGURE 4. Flowchart of the use of the (G)IA. Better results are obtained using the so-called continuation method: the number of DoF are increased gradually while imposing tighter and tighter constraints on the radiated field until a satisfactory result is obtained.

#### D. PRACTICAL USE OF THE GIA ALGORITHM

The use of optimization algorithms for shaped-beam antenna design is rarely a straight task. Antenna and radiated field specifications need to be defined beforehand and then implemented into the optimization algorithm. Moreover, a single instance of the optimization process may yield suboptimal results, especially for applications that require arrays with hundreds or even thousands of elements with stringent requirements on the radiated field. A more suitable approach is then the so-called continuation method [35]: divide the synthesis procedure into several steps, gradually increasing the number of DoF and tightening constraints until a satisfactory result is obtained.

This approach is illustrated in FIGURE 4, where at each stage the GIA is run a variable number of iterations that will depend on the number of DoF and imposed constraints. It is the decision of the designer to assess when the GIA, should have not reached convergence, will be stopped to adjust the number of DoF and constraints and run it again. Eventually, given a suitable starting point for each stage, the algorithm will converge into a suitable solution. Finally, it is worth remarking that this strategy is not only suitable for the GIA, but for any optimization algorithm.

#### E. COMPARISON WITH OTHER ALGORITHMS

As previously mentioned, the GIA arises as a solution to overcome two limitations of the classical IA, namely, the problem of local minima and the limited scope of the optimizing variables. On the one hand, local minima appear since the optimization problem is not convex, and the IA is a local optimizer. Although the GIA does not fully solve this issue, it alleviates this problem by converting one of the two sets involved in the synthesis into a convex set [35] and by employing the continuation method illustrated in FIGURE 4.

On the other hand, the scope of the optimizing variables is expanded since in the IA only variables directly related to the field at the aperture could be optimized (magnitude and/or phase of the field at the aperture of the array), while in the GIA the optimizing variables are not limited to those, but can be expanded to the geometrical features of the unit cell. This opens up the possibility of direct layout optimizations taking into account the real electromagnetic response of the array unit cell that was not possible with the classical IA, allowing, for instance, the crosspolar optimization and/or multi-frequency optimization. Some examples will be reviewed in Section V.

Compared with other algorithms in the literature, the GIA seems to offer better results, at least in the relevant case of very large arrays comprised of thousands of elements. First, global search algorithms, such as GA or PSO, have been widely employed to synthesize all kinds of arrays [36], [37], [38], [39], [40], [41]. However, these arrays are usually relatively small, comprised at most of a few hundred elements. Indeed, since the search space grows exponentially with the number of DoF (i.e., optimizing variables) and global search algorithms perform an exhaustive search, it becomes increasingly harder to achieve suitable results with larger arrays. Very few studies with limited results are available of very large arrays, comprised of thousands of elements, optimized by global search algorithms [60]. Another limitation of this class of algorithms is that they require in the order of dozens of thousands of iterations to achieve suitable shaped beams [37], [60]. This in turn limits their applicability since small increases in the evaluation of the cost function may have an important impact on their computational efficiency.

On the other hand, local search algorithms such as the LM [31], BFGS [32] or gradient minimax [42] require far fewer iterations, although at the expense of the evaluation of derivatives of a cost function, which is more computationally expensive. Although the GIA also suffers from this issue since it employs a general minimization algorithm in the backward projection, its improved convergence properties alleviates to a certain extent this issue. Indeed, the GIA has proven to provide better results when compared with other algorithms. For instance, the classical IA and GIA are compared in [49] synthesizing an antenna comprised of more than 5000 elements. While the IA fails to provide a solution, presenting a very high ripple in the coverage region, the GIA is able to provide a suitable solution. The GIA and the LM were compared in [50] in two cases: a 900-element reflectarray with a shaped pattern for local multipoint distribution system and 5180-element reflectarray for direct broadcast satellite application. In the first case, the GIA is able to offer better results in fewer iterations than the LM, while in the second case the LM fails to converge and the GIA successfully shapes the desired beam. The GIA has also been able to provide better results than other works in the literature when tackling the design of a broadband antenna with improved polarization purity for direct-to-home applications as described in [7] (compared to the classical IA [61]), and in the design of a

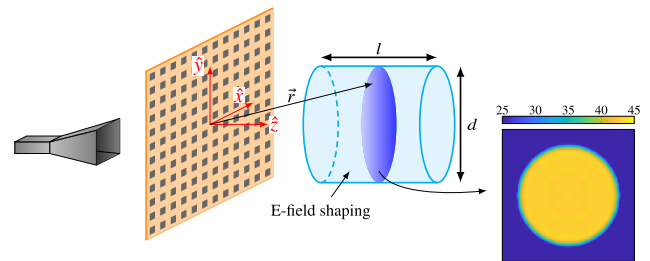


**FIGURE 5.** The first scenario consists of a transmitarray for near field shaping. The objective is to shape the near field radiated by the antenna in a volume in front of it. To that end, the volume is discretized into several planes and mask requirements are imposed in all of them.

contoured-beam dual-band reflectarray [44] (compared to the gradient minimax [6] and the classical IA [62], [63]).

#### IV. EXAMPLES OF APPLICATION

In this section we will show three relevant examples of application of the GIA to synthesize the radiated field. These examples have been chosen to showcase a variety of scenarios and arrays: a transmitarray for near field coverage, an aperiodic phased-array with an isoflux pattern to provide constant power flux in the coverage area, and a reflectarray with squared-secant pattern in elevation and sectored-beam in azimuth with improved cross-polarization performance.

In the following Subsections, concrete formulations for the field  $\vec{E}$  used throughout Sections II and III will be given, either in the near or far field region for the three types of array. The subscript  $n$  indicating a generic iteration of the algorithm is dropped in order to alleviate notation.

##### A. TRANSMITARRAY FOR CONSTANT NEAR FIELD DISTRIBUTION

###### 1) NEAR FIELD EQUATIONS FOR PLANAR TRANSMITARRAY SYNTHESIS

The first scenario is depicted in FIGURE 5. It is a transmitarray whose near field magnitude is going to be shaped to provide a wide constant power density within a certain volume in front of the antenna. The near field model employed in this case consists in the superposition of the far field generated by each transmitarray element [64]:

$$\vec{E}_{\text{nf}}(\vec{r}) = \sum_{i=1}^I \vec{E}_{\text{ff},i}(\vec{r}) = \sum_{i=1}^I \left( E_{\theta,i}(\vec{r}) \hat{\theta} + E_{\varphi,i}(\vec{r}) \right), \quad (17)$$

where  $I$  is the total number of transmitarray elements,  $\vec{r}$  is the observation point, and  $E_{\theta}$  and  $E_{\varphi}$  are the far field components that may be calculated using the second principle of equivalence in electromagnetics [48]:

$$E_{\theta,i} = \frac{jk_0 e^{-jk_0 r_i}}{2\pi r_i} (P_{x,i} \cos \varphi_i + P_{y,i} \sin \varphi_i),$$

$$E_{\varphi,i} = -\frac{jk_0 e^{-jk_0 r_i}}{2\pi r_i} \cos \theta_i (P_{x,i} \sin \varphi_i - P_{y,i} \cos \varphi_i), \quad (18)$$

where  $k_0$  is the free-space wavenumber, and  $P_{x/y,i}$  is the spectrum function of a single transmitarray element  $i$ , whose

subscript  $x/y$  indicates the tangential electric field component according to  $\hat{x}$  and  $\hat{y}$  from FIGURE 5. Each transmitarray element is modelled as a small aperture with constant field on it. Thus, the spectrum functions may be written as [65]:

$$P_{x/y,i} = E_{ap,x/y}^i a b \operatorname{sinc}\left(\frac{k_0 u_i a}{2}\right) \operatorname{sinc}\left(\frac{k_0 v_i b}{2}\right), \quad (19)$$

where the subindex indicates the tangential component of the field;  $u_i = \sin \theta_i \cos \varphi_i$ ,  $v_i = \sin \theta_i \sin \varphi_i$ ;  $a$  and  $b$  are the periodicity of the transmitarray unit cell in  $\hat{x}$  and  $\hat{y}$ , respectively. It is worth noting that this near field model based on the superposition of the far field generated by the array elements has been widely employed in the literature [55], [64], [65], [66], [67], [68] and validated through full-wave simulations with commercial software [64], [65] as well as measurement of prototypes [55], [66], [67], [68].

For this synthesis, the optimization variables will be the phase-shift introduced by the transmitarray element, which is modelled as an ideal phase-shifter. Thus, the field at the aperture may be approximated by:

$$E_{ap,x/y}^i \approx \exp(j\phi_{i,x/y}) E_{inc,x/y}^i, \quad (20)$$

where  $\phi_{i,x/y}$  is the phase-shift introduced by the  $i$ -th transmitarray element for the appropriate polarization [69], and  $E_{inc}^i$  is the incident field produced by the feed on the  $i$ -th transmitarray element. By using the notation of Section III, we can identify  $\phi_i$  for each transmitarray element as the optimizing variables of the algorithm:  $\vec{x}_k = \{\phi_i\}$ , with  $k = 1, \dots, K$ ,  $i = 1, \dots, L$ ,  $K = L$ , for a given polarization, either  $x$  or  $y$ . Thus, the propagation operator  $\mathcal{P}\{\cdot\}$  of (11) in this case can be described by (17)–(20) plus the squaring of the near field magnitude calculated by (17). In addition, constraint (8) is enforced to maintain the same magnitude of the incident field imposed by the feed.

## 2) ANTENNA AND FIELD SPECIFICATIONS

The transmitarray is made up of  $I = 3600$  elements in a regular grid of  $60 \times 60$  unit cells. The periodicity is  $a = b = 3.84$  mm in both directions, which is approximately  $0.5\lambda_0$  at the working frequency, 39 GHz. The feed is modelled with a  $\cos^q \theta$  function [70], with  $q = 22$  and placed at a distance of 180 mm using a centered configuration. The antenna aperture ( $D$ ) is  $230 \times 230$  mm<sup>2</sup> ( $\sim 894\lambda_0^2$ ) and the volume where the field distribution should be constant is a cylinder with radius 175 mm ( $22.75\lambda_0$ ) and depth 100 mm ( $13\lambda_0$ ), starting at a distance  $z = 550$  mm from the transmitarray center. The requirement is set for a maximum magnitude ripple of 1 dB within the defined near field volume.

The starting point of the optimization is a far field colimated beam pointing towards the center of the volume. In addition, the optimization will be carried out in several stages to ease the convergence towards a solution, gradually increasing the number of optimizing variables. Moreover, in the first stages of the optimization, only one near field plane will be optimized, that at  $z = 600$  mm, since the field shaping will conserve its properties in other planes as well [65]. Then,

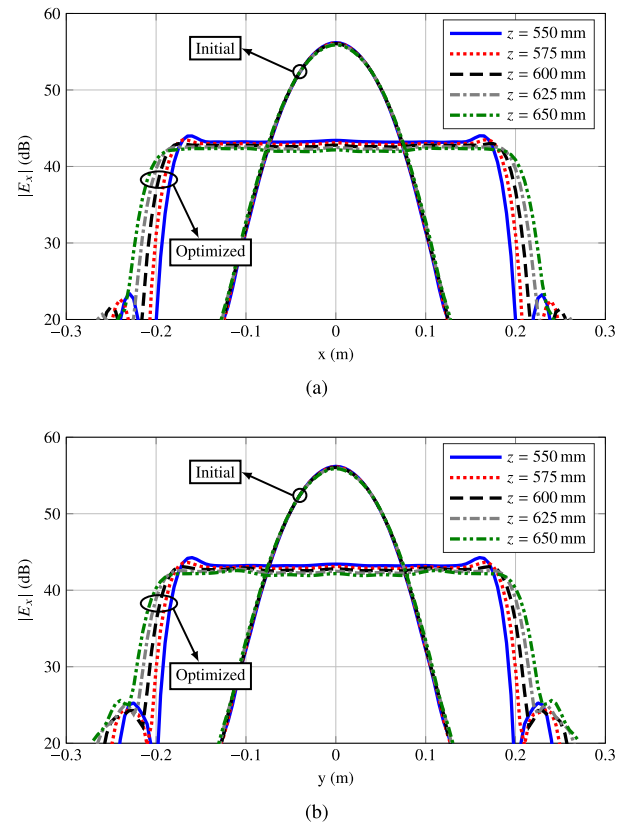


**FIGURE 6. Results of the transmitarray near field optimization to achieve a constant field distribution. Both the starting point and the optimized field are shown at different planes with constant  $z$  in front of the transmitarray. (a) Main cut for  $y = 0$ . (b) Main cut for  $x = 0$ .**

in the last stages of the optimization two more planes are added to fine tune the achieved ripple, corresponding to  $z = 550$  mm and  $z = 650$  mm. After the optimization, a total of five planes within the region of interest will be evaluated.

## 3) RESULTS

FIGURE 6 shows the main cuts ( $x = 0$  mm and  $y = 0$  mm) of the near field magnitude before and after the phase-only optimization for five different planes within the previously defined cylindrical volume. As can be seen, the optimized near field clearly satisfies the imposed specifications and a constant field distribution is achieved within the volume. Moreover, the diameter of the coverage area with a ripple of 1 dB is increased from the 40 mm of the starting point to the 350 mm of the optimized field. This is an increment of more than 700%. For each plane, the size of the area with a 1 dB ripple is approximately improved by more than a factor of 70. In addition, a side lobe level of around 16 dB is achieved outside the coverage area. Finally, FIGURE 5 also shows the achieved circular field coverage in the plane  $z = 600$  mm.

## B. APERIODIC PHASED-ARRAY WITH ISOFLUX PATTERN

### 1) FAR FIELD OF THE APERIODIC PHASED-ARRAY

The second scenario is shown in FIGURE 7, and it corresponds to a phased-array placed in a satellite in geostationary



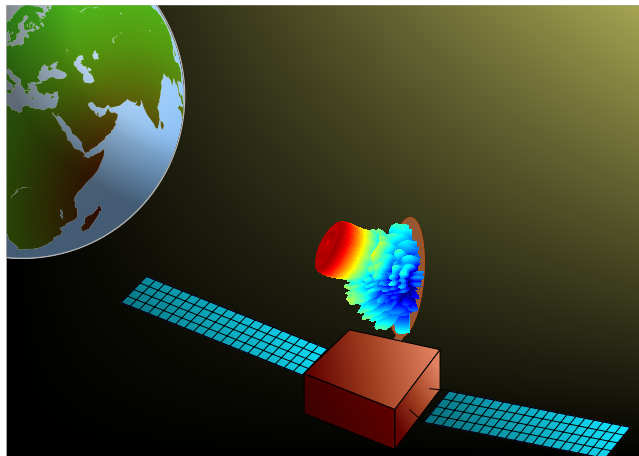


**FIGURE 7.** The second scenario is of an aperiodic phased-array that generates an isoflux pattern for global Earth coverage from a geostationary orbit. To that end, a phase-only synthesis is carried out that models the element as an ideal phase-shifter, i.e., with no losses and no cross-polarization. Drawing not to scale.

orbit to provide global Earth coverage by means of an isoflux pattern. For this case we consider the far field as the array factor of the aperiodic phased-array as:

$$\vec{E}_{\text{ff}} = \sum_{i=1}^I E_{\text{ap}}^i \exp [j(x_i k_x + y_i k_y)], \quad (21)$$

where  $(x_i, y_i)$  are the coordinates of each array element, and  $k_x = uk_0$ ,  $k_y = vk_0$ . For the phased-array the magnitude of the field at the aperture ( $|E_{\text{ap}}^i|$ ) will be constant, and the optimizing variables will be  $\vec{x}_k = \{\angle E_{\text{ap}}^i\}$ ,  $k = 1, \dots, K$ ,  $i = 1, \dots, L$ ,  $K = L$ . No constraints will be imposed to the optimizing variables.

## 2) ANTENNA AND FIELD SPECIFICATIONS

The aperiodic distribution of the elements is achieved by following the strategy described in [71], which requires an initial periodic array. In this case, we consider a periodic square array of  $44 \times 44$  elements with a periodicity of  $0.4\lambda_0$  in both directions. The initial excitation follows a raised cosine distribution. Then, the obtained aperiodic array presents a uniform excitation (i.e.,  $|E_{\text{ap}}^i| = 1, \forall i$ ) and it is made up of  $I = 1444$  elements in a grid of  $38 \times 38$ . In addition, the periodicity profile varies between  $0.4\lambda_0$  and  $0.6\lambda_0$ , which avoids the appearance of pseudo-grating lobes. The working frequency is 30 GHz. For the isoflux pattern, specifications include a ripple in the coverage area of 0.2 dB and a maximum side lobe level (SLL) of  $-19$  dB.

## 3) RESULTS

For this example, in addition to a gradual increase of the optimizing variables in subsequent stages, the mask requirements are also modified. Starting with an allowable ripple of 0.75 dB, it is decreased until a ripple of 0.2 dB is achieved in the final radiation pattern. In this way, convergence of the algorithm is facilitated. FIGURE 8 shows the results for the

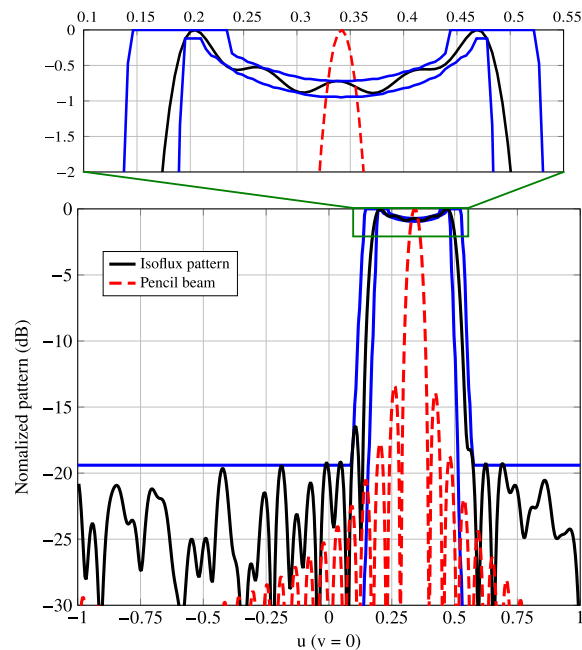


**FIGURE 8.** Results of the aperiodic phased-array optimization to achieve an isoflux pattern for global Earth coverage. The starting point for the optimization was the pencil beam. The optimized isoflux pattern achieves a ripple in the coverage area of 0.2 dB and a SLL of  $-19$  dB.

optimization of the aperiodic phased-array. The starting point of the optimization was a collimated beam radiating towards the center of the coverage area, which corresponds to  $u = \sin 20^\circ \approx 0.34$  (for  $v = 0$ ). After the phase-only synthesis, the isoflux pattern complies with the imposed specifications in both ripple and SLL.

## C. DIRECT LAYOUT OPTIMIZATION OF A REFLECTARRAY ANTENNA

### 1) FAR FIELD RADIATED BY THE REFLECTARRAY

The third scenario, shown in FIGURE 9, consists of a single offset-fed reflectarray with a squared-secant pattern in elevation and sectored-beam in azimuth with improved crosspolarization performance to provide coverage for 5G base stations at 28 GHz. Now, we consider the copolar ( $E_{\text{co}}$ ) and crosspolar ( $E_{\text{xp}}$ ) components of the far field given by Ludwig's third definition [72]:

$$\begin{aligned} E_{\text{co}} &= \sin \varphi E_{\theta} + \cos \varphi E_{\varphi}, \\ E_{\text{xp}} &= \cos \varphi E_{\theta} - \sin \varphi E_{\varphi}, \end{aligned} \quad (22)$$

where  $E_{\theta}$  and  $E_{\varphi}$  are defined in (18). For the reflectarray, the spectrum function takes the form:

$$P_{x/y} = K \sum_{i=1}^I E_{\text{ap},x/y}^i \exp [j(x_i k_x + y_i k_y)], \quad (23)$$

where  $K$  is a constant:

$$K = ab \operatorname{sinc} \left( \frac{k_0 u_i a}{2} \right) \operatorname{sinc} \left( \frac{k_0 v_i b}{2} \right). \quad (24)$$

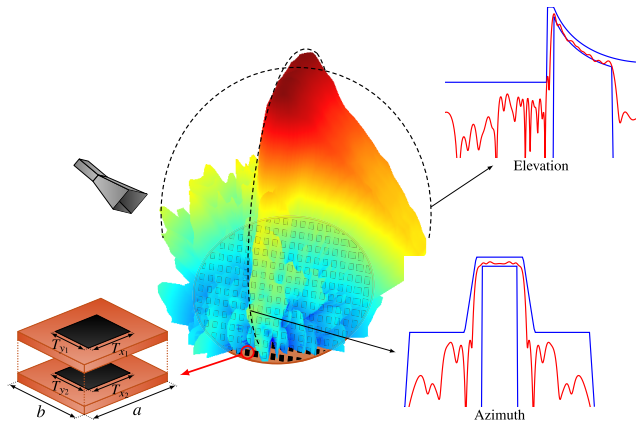


**FIGURE 9.** In the third scenario, a reflectarray antenna layout is optimized to achieve a squared-cosecant pattern in elevation and sectored-beam in azimuth with improved cross-polarization performance. This is done by modelling the unit cell with a method of moments tool, which is directly employed in the optimization loop in the backward projection.

Please note that now we are calculating the spectrum function for the whole reflectarray antenna, while in (19) it was done for a single transmitarray element.

The field at the aperture for each reflectarray element can be obtained from the incident field imposed by the feed and the matrix of reflection coefficients that describe the electromagnetic response of the reflectarray unit cell [73]:

$$\begin{pmatrix} E_{ap,x}^i \\ E_{ap,y}^i \end{pmatrix} = \begin{pmatrix} \rho_{xx}^i & \rho_{xy}^i \\ \rho_{yx}^i & \rho_{yy}^i \end{pmatrix} \begin{pmatrix} E_{inc,x}^i \\ E_{inc,y}^i \end{pmatrix}. \quad (25)$$

While  $E_{inc}$  is fixed and imposed by the feed, the reflection coefficients depend on several parameters: working frequency, substrate characteristics, periodicity, angle of incidence and unit cell geometric features. From all of these, only the geometrical features vary, while the rest remain fixed. In the present case, a unit cell comprised of two stacked rectangular patches are employed, with dimensions  $T_{x1}$  and  $T_{y1}$  for the top layer, and  $T_{x2}$  and  $T_{y2}$  for the bottom layer. The dimensions of the patches will be employed as optimizing variables. Thus,  $\vec{x}_k = \{T_{x1}^i, T_{y1}^i, T_{x2}^i, T_{y2}^i\}$ ,  $i = 1, \dots, I$ ,  $k = 1, \dots, K$ ,  $K = 4I$ . Moreover, in this case, constraints on  $\vec{x}_k$  are imposed, specifically those of (16) so that the dimensions of the patches are positive and smaller than the periodicity of the unit cell.

Finally, it is worth mentioning that the reflection coefficients are computed by the method of moments based on local periodicity described in [74].

## 2) ANTENNA AND FIELD SPECIFICATIONS

The considered reflectarray is circular and comprised of  $I = 912$  elements distributed in a regular grid of 34 elements in the main axes. The periodicity is  $a = b = 0.5\lambda_0$  at the working frequency (28 GHz) and the feed is modelled with a  $\cos^q \theta$  function, generating an illumination taper of  $-14.6$  dB. The feed is placed at  $(-79.3, 0.0, 200.2)$  mm with regard to the reflectarray center. The same substrate is used in

**TABLE 1.** Summary of the performance for the reflectarray for 5G base stations regarding the crosspolarization improvement using the GIA for a direct layout optimization.

	CP <sub>max</sub>	XP <sub>max</sub>	CP <sub>max</sub> -XP <sub>max</sub>
After POS	19.6 dBi	-6.1 dBi	25.7 dB
After XP opt.	19.7 dBi	-15.7 dBi	35.4 dB

both layers of the unit cell, with relative permittivity of 3 and a loss tangent of 0.001, which corresponds to the commercially available Rogers R3003. In addition, the bottom layer has a thickness of 30 mil, while the top layer has a thickness of 20 mil. Regarding the far field specifications, the chosen pattern for the 5G base station has a  $30^\circ$  sectored beam in azimuth and a squared-cosecant beam in elevation to provide constant power flux in an elevation span of  $50^\circ$ .

The process to design this antenna is divided into three steps, two of which employ the GIA algorithm. First, a POS is carried out with the GIA to obtain the required phase-shift to radiate the desired far field. In the second step, a layout is obtained by adjusting the unit cell geometry to match the synthesized phases. And third, the layout is optimized with the GIA to improve crosspolarization performance while maintaining the copolar pattern requirements. A detailed explanation of this procedure may be found in [75].

## 3) RESULTS

The radiation patterns before and after the direct layout optimization for cross-polarization improvement are shown in FIGURE 10. It can be seen that the side lobe level is slightly worse after the crosspolar optimization. However, this small deterioration in the copolar pattern is compensated by the improvement in cross-polarization performance. This is assessed by the maximum copolar gain/maximum crosspolar gain ratio (CP<sub>max</sub>/XP<sub>max</sub>). It is defined, in logarithmic scale, as the difference between the maximum copolar gain and the maximum crosspolar gain. TABLE 1 shows the improvement in cross-polarization performance after the direct layout optimization. XP<sub>max</sub> decreases more than 9 dB while maintaining the copolar gain and mostly complying with the specifications, as shown in FIGURE 10.

## D. SOME PROTOTYPES DESIGNED WITH THE (G)IA

The three previous examples showcase the capabilities of the GIA to achieve near and far field shaping of different types of arrays. Although the examples are based only on simulations, the (G)IA has been used with success to design different types of antenna prototypes whose measurements agree satisfactorily with the prediction of the simulations. A small selection follows.

A dual-polarization dual-coverage reflectarray for space applications was design, manufactured and measured in [5] using the IA to obtain the phase-shift introduced by the array elements. The produced shaped pattern provides European coverage in the horizontal polarization, while it illuminates

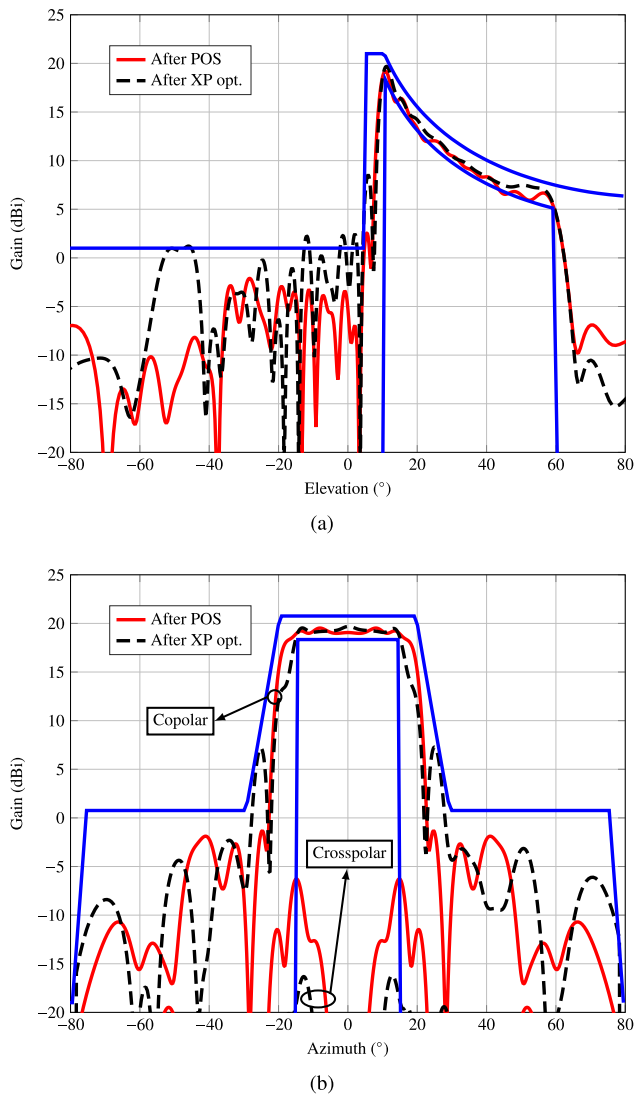


**FIGURE 10.** Main cuts of the radiation pattern at 28 GHz radiated by the reflectarray for a 5G base station with (a) a squared-cosecant pattern in elevation and (b) sectorized-beam in azimuth. It shows the results for the copolar and crosspolar patterns after the phase-only synthesis (POS) and after the crosspolar optimization, both carried out with the GIA. Due to a symmetry in the antenna optics, the crosspolar level in the elevation cut is very low and out of range.

the North American east coast in vertical polarization. Another reflectarray was designed with the IA in [11] to produce three beams for a local multipoint distribution system central station antenna in the far field. In the near field, another prototype was designed in [55] with magnitude and phase constraints to work as a compact antenna test probe for 5G new radio devices. Two reflectarray prototypes identical in size were designed using the GIA, manufactured and tested achieving a good trade-off between the performance and the low-cost, low losses and low-profile characteristics in [76]. The IA has also been used with success to design a 3D printed transmitarray with a shaped near field for wireless power transfer [68]. More examples may be found in the literature review carried out in Section V.

## V. LITERATURE REVIEW OF THE INTERSECTION APPROACH

### A. THE MULTIPLE NAMES OF THE METHOD

In this work, we have been employing the name of intersection approach (IA) for the algorithm described in Sections II and III. However, in the literature it is also known as alternate projection algorithm (APA) or alternate projection method (APM). This comes from the fact that the goal of this algorithm is to find the intersection between two or more sets, hence *intersection approach*. To that end, it iteratively and alternately applies two projections to find such intersection, hence the names *alternate projection algorithm* or *method*. A particular implementation of the two projectors for linear and planar arrays allows the application of the FFT algorithm for a fast synthesis process. Thus, some authors call this method *iterative Fourier technique* (IFT) based on the application of successive fast Fourier transforms.

### B. EARLY DEVELOPMENT OF THE IA

The idea of solving the pattern synthesis problem as the intersection between two or more sets by using an iterative algorithm based on alternate projections can be traced back to the early 1970s to the Russian school [77], as cited in [78, p. 1018]. In addition, [79] is mentioned in [80] as an iterative method based on the evaluation of stationary phase patterns that achieves exactly the same results as the method of projections [30] if the same starting point is used. The projection method [77] was later extended to non-uniform arrays in [81]. Around that time in the early 1980s, Prasad applied the alternative orthogonal projection algorithm for the synthesis of null-steering patterns [82], which was later improved by Kumar [83] and Ng [84] for the null-steering problem. It was later applied by Poulton for the power pattern synthesis of contoured-beam arrays [85] and the synthesis of plane waves in the near field [86].

It was mentioned in [87] that Carroll and Kumar were the first to apply the FFT algorithm to perform the successive projections for array pattern synthesis [88]. Their technique was based on the Gerchberg-Saxton error reduction algorithm [89] for image reconstruction. However, Bucci *et al.* introduced the concept earlier for pattern synthesis [90], [91], in which the far field at a certain iteration is transformed with the FFT, then truncated to the source domain (since the number of points in both domains may be different but the FFT requires the same number of points in both domains), and then the far field for the new iteration is obtained again with the FFT [91].

Nevertheless, it was not until the early 1990s that the algorithm was popularized by Bucci *et al.* in a series of papers [30], [92], [93], [94] where they further developed, improved and applied the algorithm for array pattern synthesis with constraints, shaped reflector antennas and reconfigurable arrays by phase-only control. They later generalized the methodology in [35] to consider the full synthesis problem independently of the actual structure of the antenna.

### C. APPLICATIONS OF THE IA IN THE LITERATURE

Since the early days of the intersection approach developments in its various forms, as described above, many authors have extended, improved and used the algorithm for the synthesis of several antenna types, mostly arrays. This involves the particularization of both projections in (1) and (10) to the considered antenna and its mathematical analysis.

One attractive feature of the algorithm is that, in its classical implementation [30], [88], the projections are implemented with the FFT algorithm, resulting in a very computationally efficient algorithm for pattern synthesis. This is possible since the far field can be obtained as the Fourier transform of the tangential field at the aperture [48]. Thus, the IA has found applications for the synthesis of very large arrays. For instance, in [51] Zornoza and Encinar particularize the IA for very large reflectarray antennas. In order to improve convergence, they adopt a fictitious reduction of variables by modifying the illumination taper of the feed in successive stages. This algorithm was then used for the design of several very large, contoured-beam reflectarrays for space applications [5], [62], [95], [96], base stations [11] or global Earth coverage [97]. Keizer applies the algorithm to very large arrays for low-sidelobe pattern synthesis of dense [98], [99], [100] and thinned [101] arrays, to correct for element failures [102], linear [103] and planar [104], [105] array thinning. Other works have also tackled the synthesis of thinned arrays with the IA [106], [107], [108], [109]. The IA is improved in [110] to include the effect of different incidence angles on the reflectarray elements in the evaluation of the design curve. To that end, phase and magnitude curves are precomputed for a few incidence angles and the backward projector is accordingly modified to take those curves into account. Some works have employed adaptive masks to improve convergence [111], [112], where the mask applied in the forward projection changes its level with regard to the radiated field at every iteration.

Although employing the FFT in both projections presents the advantage of computational efficiency, it presents some drawbacks for advanced array synthesis. On the one hand, using the FFT in the backward projector to recover the tangential field at the aperture means that the optimizing variables will be those directly related to such field, i.e. the complex excitation in arrays, or phase-shift in phased-arrays, reflectarrays or transmitarrays. This in turn limits the optimization to the copolar pattern, since the crosspolar pattern cannot be properly characterized without the effect of the real element. On the other hand, it is known that the IA presents the problem of local minima which mainly depends on two factors: the number of degrees of freedom employed in the synthesis and the non-convexity of the sets [35]. The latter issue may be overcome by considering the squared field magnitude or gain for a power pattern synthesis, as suggested in [35]. Both methods (i.e. considering the field magnitude vs. the squared field magnitude) were compared in [49], where it was shown that the power pattern synthesis with the squared field magnitude offers superior results. However, in this case

the FFT cannot be employed to recover the tangential field and a general minimization algorithm must be used, penalizing computational efficiency in the interest of better convergence properties. This was the methodology followed in [113] and [114] for the synthesis of conformal arrays and in [115], [116], and [117] for the crosspolar optimization of reflectarray antennas along with a MoM-LP for the element simulation. In those works, the BFGS algorithm is used in the backward projection.

Due to the low computational efficiency of using a general minimization algorithm such as the BFGS and a MoM-LP tool within the optimization loop, some techniques have been introduced to improve efficiency of the generalized IA (GIA). For instance, in [24] the LM algorithm is used in the backward projection with a technique that allows to minimize the number of MoM-LP calls in the computation of the Jacobian matrix. Another technique to improve the computational efficiency is the differential contributions (DFC), which is based on the linearity of Maxwell's equations, leading to a linear dependence between the field in the aperture and the radiated field (either near field or far field). This in turn allows to accelerate the computation of the gradient (i.e. Jacobian or Hessian matrix in the LM or BFGS, respectively) [118]. The MoM-LP tool may be substituted by surrogate models of the unit cell, considerably accelerating the overall synthesis process [75], [119]. Alternatively, databases may also be employed [120].

These techniques were integrated in the GIA in [7] to synthesize a broadband contoured-beam reflectarray with 20% bandwidth and improved cross-polarization performance for space applications. In [44] a multi-stage multi-objective GIA was employed to design a transmit-receive reflectarray, outperforming earlier works in the literature. Furthermore, the forward projector may be improved to optimize some figure of merit other than the copolar or crosspolar patterns in far field applications. For instance, in [121] it is suggested to improve cross-polarization performance of reflectarray antennas by directly optimizing the crosspolar discrimination or crosspolar isolation parameters. Equivalently, in [44] the minimum copolar gain at each coverage area is optimized instead of the copolar pattern in a given  $u$ - $v$  region. As a positive side effect, the optimization of these figures of merit allows to improve the computational performance of the GIA by accelerating computations and reducing memory usage.

The previous works have employed the (G)IA for the synthesis of different antennas in the far field. However, it can also be employed for near field synthesis. The FFT can still be applied in this context in both the forward and backward projectors by expressing the near fields in terms of their plane wave spectrum [47]. Ettore *et al.* follow this approach for shaping the near field of a radial line slot array on a plane [122], on a volume [123], as well as the near field of a metasurface [124]. A similar idea is applied in [125] to obtain a quasi-constant power density in the near field using a reflector antenna, in [46] for a plane wave generator and in [126] for a programmable reflective metasurface to

emulate real fields. A different and novel approach for the POS of the near-field in transmitarray antennas consists in calculating, as an intermediate step, the far field radiated by the truncated near field after applying the forward projection, and then recovering the field at the aperture [68]. This process is repeated until the desired near field is achieved. The GIA was also applied to the near field synthesis of reflectarray antennas [55], [127], [128]. A combined near field-far field synthesis can also be carried out using the GIA framework, in which constraints are imposed in near fields planes in addition to far field specifications. This was shown in [129] for a reconfigurable conformal array, where the functional was modified to include both near and far field requirements plus a coefficient to weight the relative relevance of both fields.

### D. FUTURE APPLICATIONS OF THE INTERSECTION APPROACH

As new antenna applications arise with ever stringent requirements, so the use of the (G)IA may be extended to improve the performance of those antennas. Some recent novel applications include the extensive research on dual-band dual circularly-polarized (CP) arrays for high-throughput communications. Reflectarrays are of particular interest since they may provide multispot coverage with a smaller number of apertures in the K and Ka bands [130]. In this regard, the GIA may be employed to optimize cross-polarization levels in dual-CP planar [130] or curved reflectarrays [131]. Dual-CP shaped-beam reflectarrays are also a novel topic that has not been addressed in the literature yet.

Regarding applications in the near field, intelligent reflective surfaces are a novel technology that aim at improving the performance of wireless data transmission systems [132]. In addition to shaping the near field copolar pattern, cross-polarization improvement in the near field still remains to be addressed. Moreover, when tackling cross-polarization improvement over a bandwidth, the surrounding walls may also need to be included in the optimization procedure to account for the effects of the scattered field by the wall. The (G)IA could be employed for this application given its potential for near field syntheses as shown in this work.

### VI. CONCLUSION

We have presented the generalized Intersection Approach (GIA) as an extension of the classical IA in which the backward projection is implemented by a general optimization algorithm. The GIA improves the IA in two aspects: it minimizes the number of local minima by working with the squared field magnitude, turning set  $\mathcal{R}$  into a convex set and thus improving convergence of the algorithm. The use of a general optimization algorithm in the backward projection allows to extend the capabilities of the algorithm, allowing to expand the scope of the optimizing variables allowing, for instance, to perform direct layout optimizations, useful to tackle wideband and crosspolar optimization of array antennas. The versatility of the GIA for array synthesis has

been shown through a selection of three relevant examples: a transmitarray for near field shaping, an aperiodic phased-array with an isoflux pattern and a direct layout optimization of a reflectarray antenna for copolar and crosspolar optimization. Finally, a thorough literature review of the use of the (G)IA is provided, accounting for the early years of development, extensions and improvements in various works to the backward and forward projection to achieve new features in addition to current use for the synthesis of different types of antennas.

### ACKNOWLEDGMENT

The author would like to thank Dr. A. F. Vaquero, Mr. B. Imaz-Lueje, Dr. M. Arrebola, and Dr. M. R. Pino for the fruitful discussions on array optimization in general, and on the intersection approach in particular.

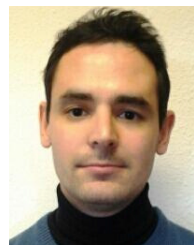
### REFERENCES

- [1] D.-W. Duan and Y. Rahmat-Samii, "A generalized diffraction synthesis technique for high performance reflector antennas," *IEEE Trans. Antennas Propag.*, vol. 43, no. 1, pp. 27–40, Jan. 1995.
- [2] J. E. Richie and H. N. Kritikos, "Linear program synthesis for direct broadcast satellite phased arrays," *IEEE Trans. Antennas Propag.*, vol. AP-36, no. 3, pp. 345–348, Mar. 1988.
- [3] L. de Haro, J. L. Besada, and B. Galocha, "On the radiation of horn clusters including mutual coupling and the effects of finite metal plates: Application to the synthesis of contoured beam antennas," *IEEE Trans. Antennas Propag.*, vol. 41, no. 6, pp. 713–722, Jun. 1993.
- [4] D. M. Pozar, S. D. Targonski, and R. Pokuls, "A shaped-beam microstrip patch reflectarray," *IEEE Trans. Antennas Propag.*, vol. 47, no. 7, pp. 1167–1173, Jul. 1999.
- [5] J. A. Encinar, L. S. Datashvili, J. A. Zornoza, M. Arrebola, M. Sierra-Castaner, J. L. Besada-Sanmartin, H. Baier, and H. Legay, "Dual-polarization dual-coverage reflectarray for space applications," *IEEE Trans. Antennas Propag.*, vol. 54, no. 10, pp. 2827–2837, Oct. 2006.
- [6] M. Zhou, O. Borries, and E. Jørgensen, "Design and optimization of a single-layer planar transmit-receive contoured beam reflectarray with enhanced performance," *IEEE Trans. Antennas Propag.*, vol. 63, no. 3, pp. 1247–1254, Apr. 2015.
- [7] D. R. Prado, M. Arrebola, M. R. Pino, and G. Goussetis, "Broadband reflectarray with high polarization purity for 4K and 8K UHD TV DVB-S2," *IEEE Access*, vol. 8, pp. 100712–100720, 2020.
- [8] E. L. Holzman, "Pillbox antenna design for millimeter-wave base-station applications," *IEEE Antennas Propag. Mag.*, vol. 45, no. 1, pp. 27–37, Feb. 2003.
- [9] L. Freytag and B. Jecko, "Cosecant-squared pattern antenna for base station at 40 GHz," in *Proc. IEEE Antennas Propag. Soc. Symp.*, Jun. 2004, pp. 2464–2467.
- [10] J. A. Martinez-Lorenzo, M. Arias, O. Rubinos, J. Gutierrez, and A. Garcia-Pino, "A shaped and reconfigurable reflector antenna with sectorial beams for LMDS base station," *IEEE Trans. Antennas Propag.*, vol. 54, no. 4, pp. 1346–1349, Apr. 2006.
- [11] M. Arrebola, J. A. Encinar, and M. Barba, "Multifed printed reflectarray with three simultaneous shaped beams for LMDS central station antenna," *IEEE Trans. Antennas Propag.*, vol. 56, no. 6, pp. 1518–1527, Jun. 2008.
- [12] E. Carrasco, M. Arrebola, J. A. Encinar, and M. Barba, "Demonstration of a shaped beam reflectarray using aperture-coupled delay lines for LMDS central station antenna," *IEEE Trans. Antennas Propag.*, vol. 56, no. 10, pp. 3103–3111, Oct. 2008.
- [13] M. Koubeissi, L. Freytag, C. Decroze, and T. Monediere, "Design of a cosecant-squared pattern antenna fed by a new Butler matrix topology for base station at 42 GHz," *IEEE Antennas Wireless Propag. Lett.*, vol. 7, pp. 354–357, 2008.
- [14] M. Lanza, J. R. Perez, I. Lopez, and J. Basterrechea, "Synthesis of planar arrays using particle swarms with selection," in *Proc. VTC Spring IEEE 69th Veh. Technol. Conf.*, Apr. 2009, pp. 1–5.

- [15] D. R. Prado, J. Álvarez, M. Arrebola, M. R. Pino, R. G. Ayestarán, and F. Las-Heras, "Efficient, accurate and scalable reflectarray phase-only synthesis based on the Levenberg–Marquardt algorithm," *Appl. Comput. Electromagn. Soc. J.*, vol. 30, no. 12, pp. 1246–1255, Dec. 2015.
- [16] C. Sacchi, T. F. Rahman, N. Bartolomei, S. Morosi, A. Mazzinghi, and F. Ciabini, "Design and assessment of a CE-OFDM-based mm-wave 5G communication system," in *Proc. IEEE Globecom Workshops (GC Wkshps)*, Dec. 2016, pp. 1–7.
- [17] L.-R. Kuo, H.-T. Chou, and S.-J. Chou, "Shaped reflector antennas for outdoor BTS of 4G/5G mobile communications," in *Proc. IEEE Wireless Power Transf. Conf. (WPTC)*, May 2017, pp. 1–3.
- [18] Z.-C. Hao and M. He, "Developing millimeter-wave planar antenna with a cosecant squared pattern," *IEEE Trans. Antennas Propag.*, vol. 65, no. 10, pp. 5565–5570, Oct. 2017.
- [19] K. Quzwain, Y. Yamada, K. Kamardin, N. H. A. Rahman, and T. A. Rahman, "Design of shaped offset dual-reflector antenna for 5G mobile base station," in *Proc. IEEE Int. RF Microw. Conf. (RFM)*, Dec. 2018, pp. 5–8.
- [20] L. A. Greda, A. Winterstein, D. L. Lemes, and M. V. T. Heckler, "Beamsteering and beamshaping using a linear antenna array based on particle swarm optimization," *IEEE Access*, vol. 7, pp. 141562–141573, 2019.
- [21] D. R. Prado, J. A. Lopez-Fernandez, M. Arrebola, and G. Goussetis, "Efficient shaped-beam reflectarray design using machine learning techniques," in *Proc. 15th Eur. Radar Conf. (EuRAD)*, Sep. 2018, pp. 1545–1548.
- [22] S. Mercader-Pellicer, G. Goussetis, G. M. Medero, H. Legay, D. Bresciani, and N. J. G. Fonseca, "Cross-polarization reduction of linear-to-circular polarizing reflective surfaces," *IEEE Antennas Wireless Propag. Lett.*, vol. 18, no. 7, pp. 1527–1531, Jul. 2019.
- [23] M. Zhou, M. F. Palvig, S. B. Sorensen, J. R. D. Lasson, D. M. Alvarez, M. Notter, and D. Schobert, "Design of Ka-band reflectarray antennas for high resolution SAR instrument," in *Proc. 14th Eur. Conf. Antennas Propag. (EuCAP)*, Mar. 2020, pp. 1–5.
- [24] D. R. Prado, M. Arrebola, M. R. Pino, R. Florencio, R. R. Boix, J. A. Encinar, and F. Las-Heras, "Efficient crosspolar optimization of shaped-beam dual-polarized reflectarrays using full-wave analysis for the antenna element characterization," *IEEE Trans. Antennas Propag.*, vol. 65, no. 2, pp. 623–635, Feb. 2017.
- [25] P. M. Woodward, "A method of calculating the field over a plane aperture required to produce a given polar diagram," *J. Inst. Elect. Eng.-III, Radiolocation*, vol. 93, no. 10, pp. 1554–1558, 1946.
- [26] D. Barbiere, "A method for calculating the current distribution of Tschebyscheff arrays," *Proc. IRE*, vol. 40, no. 1, pp. 78–82, Jan. 1952.
- [27] A. Chakraborty, B. N. Das, and G. S. Sanyal, "Beam shaping using nonlinear phase distribution in a uniformly spaced array," *IEEE Trans. Antennas Propag.*, vol. AP-30, no. 5, pp. 1031–1034, Sep. 1982.
- [28] J. Perini, "Note on antenna pattern synthesis using numerical iterative methods," *IEEE Trans. Antennas Propag.*, vol. AP-19, no. 2, pp. 284–286, Mar. 1971.
- [29] T. S. Fong and R. A. Birgenheier, "Method of conjugate gradients for antenna pattern synthesis," *Radio Sci.*, vol. 6, no. 12, pp. 1123–1130, Dec. 1971.
- [30] O. M. Bucci, G. Franceschetti, G. Mazzarella, and G. Panariello, "Intersection approach to array pattern synthesis," *IEE Proc.-H Microw., Antennas Propag.*, vol. 137, no. 6, pp. 349–357, Dec. 1990.
- [31] T. H. Ismail, D. I. Abu-Al-Nadi, and M. J. Mismar, "Phase-only control for antenna pattern synthesis of linear arrays using the Levenberg–Marquardt algorithm," *Electromagnetics*, vol. 24, no. 7, pp. 555–564, Jan. 2004.
- [32] Y. Zhang, Z. Zhao, J. Wang, and G. Dan, "Antenna array beam pattern synthesis based on trust region method," in *Proc. IEEE 17th Int. Conf. Comput. Sci. Eng.*, Dec. 2014, pp. 859–862.
- [33] G. A. F. Seber and C. J. Wild, *Nonlinear Regression*. Hoboken, NJ, USA: Wiley, 2003.
- [34] J. Nocedal and S. J. Wright, *Numerical Optimization*, 2nd ed. New York, NY, USA: Springer, 2006.
- [35] O. Bucci, G. D'Elia, G. Mazzarella, and G. Panariello, "Antenna pattern synthesis: A new general approach," *Proc. IEEE*, vol. 82, no. 3, pp. 358–371, Mar. 1994.
- [36] J. M. Johnson and Y. Rahmat-Samii, "Genetic algorithm optimization and its application to antenna design," in *Proc. Antennas Propag. Soc. Int. Symp.*, vol. 1. Seattle, WA, USA, Jun. 1994, pp. 326–329.
- [37] P. Nayeri, F. Yang, and A. Z. Elsherbeni, "Design of single-feed reflectarray antennas with asymmetric multiple beams using the particle swarm optimization method," *IEEE Trans. Antennas Propag.*, vol. 61, no. 9, pp. 4598–4605, Sep. 2013.
- [38] O. Quevedo-Teruel and E. Rajo-Iglesias, "Ant colony optimization in thinned array synthesis with minimum sidelobe level," *IEEE Antennas Wireless Propag. Lett.*, vol. 5, pp. 349–352, 2006.
- [39] T. Datta and I. S. Misra, "A comparative study of optimization techniques in adaptive antenna array processing: The bacteria-foraging algorithm and particle-swarm optimization," *IEEE Antennas Propag. Mag.*, vol. 51, no. 6, pp. 69–81, Dec. 2009.
- [40] F. Ares, S. R. Rengarajan, E. Villaneuva, E. Skochinski, and E. Moreno, "Application of genetic algorithms and simulated annealing technique in optimising the aperture distributions of antenna array patterns," *Electron. Lett.*, vol. 32, no. 3, pp. 148–149, Feb. 1996.
- [41] D. W. Boeringer and D. H. Werner, "Particle swarm optimization versus genetic algorithms for phased array synthesis," *IEEE Trans. Antennas Propag.*, vol. 52, no. 3, pp. 771–779, Mar. 2004.
- [42] M. Zhou, S. B. Sørensen, O. S. Kim, E. Jørgensen, P. Meincke, and O. Breinbjerg, "Direct optimization of printed reflectarrays for contoured beam satellite antenna applications," *IEEE Trans. Antennas Propag.*, vol. 61, no. 4, pp. 1995–2004, Apr. 2013.
- [43] V. Richard, R. Loison, R. Gillard, H. Legay, M. Romier, J.-P. Martinaud, D. Bresciani, and F. Delepaux, "Spherical mapping of the second-order Phoenix cell for unbounded direct reflectarray copolar optimization," *Prog. Electromagn. Res. C*, vol. 90, pp. 109–124, 2019.
- [44] D. R. Prado, M. Arrebola, M. R. Pino, and G. Goussetis, "Contoured-beam dual-band dual-linear polarized reflectarray design using a multiobjective multistage optimization," *IEEE Trans. Antennas Propag.*, vol. 68, no. 11, pp. 7682–7687, Nov. 2020.
- [45] D. R. Prado, M. Arrebola, M. R. Pino, and F. Las-Heras, "Complex reflection coefficient synthesis applied to dual-polarized reflectarrays with cross-polar requirements," *IEEE Trans. Antennas Propag.*, vol. 63, no. 9, pp. 3897–3907, Sep. 2015.
- [46] Y. Wu, J. Wu, and Z. Li, "Plane wave synthesis using near field wave spectrum transform embedded into intersection approach," in *Proc. Int. Conf. Microw. Millim. Wave Technol. (ICMMT)*. Chengdu, China, May 2018, pp. 1–3.
- [47] Y.-T. Lo and S.-W. Lee, Eds., *Antenna Handbook*, vol. 2. New York, NY, USA: Van Nostrand Reinhold, 1993.
- [48] W. L. Stutzman and G. A. Thiele, *Antenna Theory Design*, 3rd ed. Hoboken, NJ, USA: Wiley, 2012.
- [49] A. Capozzoli, C. Curcio, A. Liseno, and G. Toso, "Fast, phase-only synthesis of aperiodic reflectarrays using NUFFTs and CUDA," *Prog. Electromagn. Res. A*, vol. 156, pp. 83–103, 2016.
- [50] D. R. Prado, M. Arrebola, M. R. Pino, and F. Las-Heras, "Improving convergence in crosspolar optimization of reflectarray antennas," in *Proc. 11th Eur. Conf. Antennas Propag. (EuCAP)*, Mar. 2017, pp. 100–103.
- [51] J. A. Zornoza and J. A. Encinar, "Efficient phase-only synthesis of contoured-beam patterns for very large reflectarrays," *Int. J. RF Microw. Comput.-Aided Eng.*, vol. 14, no. 5, pp. 415–423, Sep. 2004.
- [52] S. Loredo, G. León, O. F. Robledo, and E. G. Plaza, "Phase-only synthesis algorithm for transmitarrays and dielectric lenses," *Appl. Comput. Electromagn. Soc. J.*, vol. 33, no. 3, pp. 259–264, Mar. 2018.
- [53] G. Minatti, S. Maci, P. D. Vita, A. Freni, and M. Sabbadini, "A circularly-polarized isoflux antenna based on anisotropic metasurface," *IEEE Trans. Antennas Propag.*, vol. 60, no. 11, pp. 4998–5009, Nov. 2012.
- [54] J. A. Encinar and J. A. Zornoza, "Three-layer printed reflectarrays for contoured beam space applications," *IEEE Trans. Antennas Propag.*, vol. 52, no. 5, pp. 1138–1148, May 2004.
- [55] A. F. Vaquero, M. Arrebola, M. R. Pino, R. Florencio, and J. A. Encinar, "Demonstration of a reflectarray with near-field amplitude and phase constraints as compact antenna test range probe for 5G new radio devices," *IEEE Trans. Antennas Propag.*, vol. 69, no. 5, pp. 2715–2726, May 2021.
- [56] O. M. Bucci, G. D'Elia, and G. Romito, "Synthesis technique for scanning and/or reconfigurable beam reflector antennas with phase-only control," *IEE Proc. Microw., Antennas Propag.*, vol. 143, no. 5, pp. 402–412, Oct. 1996.
- [57] J. A. Z. Ramírez, "Desarrollo de técnicas de diseño para reflectarrays impresos multicapa con haz conformado," Ph.D. dissertation, Dept. de Electromagnetismo y Teoría de Circuitos, Universidad Politécnica de Madrid, Madrid, Spain, 2004.

- [58] B. Imaz-Lueje, D. R. Prado, M. Arrebola, and M. R. Pino, "Reflectarray antennas: A smart solution for new generation satellite mega-constellations in space communications," *Sci. Rep.*, vol. 10, no. 1, pp. 1–13, Dec. 2020.
- [59] E. Martínez-de-Rioja, J. A. Encinar, R. Florencio, and C. Tienda, "3-D bifocal design method for dual-reflectarray configurations with application to multibeam satellite antennas in Ka-band," *IEEE Trans. Antennas Propag.*, vol. 67, no. 1, pp. 450–460, Jan. 2019.
- [60] I. López, J. R. Pérez, and J. Basterrechea, "An approach for the design of reflectarrays using CG-FFT and PSO," in *Proc. 4th Eur. Conf. Antennas Propag. (EuCAP)*. Barcelona, Spain, Apr. 2010, pp. 1–5.
- [61] J. A. Encinar, M. Arrebola, M. Dejus, and C. Jouve, "Design of a 1-metre reflectarray for DBS application with 15% bandwidth," in *Proc. 1st Eur. Conf. Antennas Propag.*, Nov. 2006, pp. 1–5.
- [62] J. A. Encinar, M. Arrebola, L. F. de la Fuente, and G. Toso, "A transmit-receive reflectarray antenna for direct broadcast satellite applications," *IEEE Trans. Antennas Propag.*, vol. 59, no. 9, pp. 3255–3264, Sep. 2011.
- [63] J. A. Encinar, R. Florencio, M. Arrebola, M. A. Salas, M. Barba, R. R. Boix, and G. Toso, "Dual-polarization reflectarray in Ku-band based on two layers of dipole-arrays for a transmit-receive satellite antenna with South American coverage," in *Proc. 11th Eur. Conf. Antennas Propag. (EuCAP)*, Mar. 2017, pp. 80–83.
- [64] H.-T. Chou, N.-N. Wang, H.-H. Chou, and J.-H. Qiu, "An effective synthesis of planar array antennas for producing near-field contoured patterns," *IEEE Trans. Antennas Propag.*, vol. 59, no. 9, pp. 3224–3233, Sep. 2011.
- [65] D. R. Prado, A. F. Vaquero, M. Arrebola, M. R. Pino, and F. Las-Heras, "General near field synthesis of reflectarray antennas for their use as probes in CATR," *Prog. Electromagn. Res.*, vol. 160, pp. 9–17, 2017.
- [66] H.-T. Chou, T.-M. Hung, N.-N. Wang, H.-H. Chou, C. Tung, and P. Nepa, "Design of a near-field focused reflectarray antenna for 2.4 GHz RFID reader applications," *IEEE Trans. Antennas Propag.*, vol. 59, no. 3, pp. 1013–1018, Mar. 2011.
- [67] J. Álvarez, "Near field multifocusing on antenna arrays via non-convex optimisation," *IET Microw., Antennas Propag.*, vol. 8, no. 10, pp. 754–764, Jul. 2014.
- [68] S. Loredo, G. Leon, and E. G. Plaza, "A fast approach to near-field synthesis of transmitarrays," *IEEE Antennas Wireless Propag. Lett.*, vol. 20, no. 5, pp. 648–652, May 2021.
- [69] A. F. Vaquero, "Development of techniques for the analysis and synthesis of spatially-fed arrays for emerging applications in near-field," Ph.D. dissertation, Dept. de Ingeniería Eléctrica, Electrónica, de Comunicaciones y de Sistemas, Universidad de Oviedo, Oviedo, Spain, Sep. 2021.
- [70] Y.-T. Lo and S.-W. Lee, Eds., *Antenna Handbook*, vol. 1. New York, NY, USA: Van Nostrand Reinhold, 1993, pp. 28–29, ch. 1.
- [71] S. Suarez, G. Leon, M. Arrebola, L. F. H. Ontanon, and F. L. H. Andres, "Experimental validation of linear aperiodic array for grating lobe suppression," *Prog. Electromagn. Res. C*, vol. 26, pp. 193–203, 2012.
- [72] A. Ludwig, "The definition of cross polarization," *IEEE Trans. Antennas Propag.*, vol. AP-21, no. 1, pp. 116–119, Jan. 1973.
- [73] J. Huang and J. A. Encinar, *Reflectarray Antennas*. Hoboken, NJ, USA: Wiley, 2008.
- [74] C. Wan and J. A. Encinar, "Efficient computation of generalized scattering matrix for analyzing multilayered periodic structures," *IEEE Trans. Antennas Propag.*, vol. 43, no. 11, pp. 1233–1242, Nov. 1995.
- [75] D. R. Prado, J. A. L. Fernández, M. Arrebola, M. R. Pino, and G. Goussetis, "General framework for the efficient optimization of reflectarray antennas for contoured beam space applications," *IEEE Access*, vol. 6, pp. 72295–72310, 2018.
- [76] B. Imaz-Lueje, A. F. Vaquero, D. R. Prado, M. R. Pino, and M. Arrebola, "Shaped-pattern reflectarray antennas for mm-wave networks using a simple cell topology," *IEEE Access*, vol. 10, pp. 12580–12591, 2022.
- [77] L. D. Bakhrakh and S. D. Kremenetskii, Eds., *The Synthesis of Radiating Systems*. Moscow, Russia: Sovetskoe Radio, 1974.
- [78] Y. I. Khurgin and V. P. Yakovlev, "Progress in the Soviet union on the theory and applications of bandlimited functions," *Proc. IEEE*, vol. 65, no. 7, pp. 1005–1029, Jul. 1977.
- [79] Y. I. Choni, "Antenna synthesis according to a given amplitude radiation pattern," *Radio Eng. Electron. Phys.*, no. 5, pp. 770–778, May 1971.
- [80] M. Comisso and R. Vescovo, "Fast iterative method of power synthesis for antenna arrays," *IEEE Trans. Antennas Propag.*, vol. 57, no. 7, pp. 1952–1962, Jul. 2009.
- [81] H. Elmikati and A. Elshohly, "Extension of projection method to nonuniformly linear antenna arrays," *IEEE Trans. Antennas Propag.*, vol. AP-32, no. 5, pp. 507–512, May 1984.
- [82] S. Prasad, "Generalized array pattern synthesis by the method of alternating orthogonal projections," *IEEE Trans. Antennas Propag.*, vol. AP-28, no. 3, pp. 328–332, May 1980.
- [83] B. V. K. V. Kumar, "A modified hyperplane method for null synthesis in an array pattern," *IEEE Trans. Antennas Propag.*, vol. AP-30, no. 3, pp. 512–516, May 1982.
- [84] T. S. Ng, "Array pattern synthesis by the method of alternating orthogonal projections: The general case," *IEE Proc. H-Microw., Antennas Propag.*, vol. 132, no. 7, pp. 451–454, Dec. 1985.
- [85] G. T. Poulton, "Antenna power pattern synthesis using method of successive projections," *Electron. Lett.*, vol. 22, no. 20, pp. 1042–1043, Sep. 1986.
- [86] G. T. Poulton, "An alternative plane wave synthesis method for fresnel-zone antenna measurements," in *Proc. Dig. Antennas Propag. Soc. Int. Symp.*, Jun. 1989, pp. 90–93.
- [87] W. P. M. N. Keizer, "Low-sidelobe pattern synthesis using iterative Fourier techniques coded in MATLAB [EM programmer's notebook]," *IEEE Antennas Propag. Mag.*, vol. 51, no. 2, pp. 137–150, Apr. 2009.
- [88] C. W. Carroll and B. V. K. V. Kumar, "Iterative Fourier transform phased array radar pattern synthesis," *Proc. SPIE*, vol. 827, pp. 73–85, Nov. 1987.
- [89] R. W. Gerchberg, "A practical algorithm for the determination of phase from image and diffraction plane pictures," *Optik*, vol. 35, no. 2, pp. 237–246, 1972.
- [90] O. M. Bucci, G. D'Elia, and R. Pierri, "An efficient approach to the antenna power synthesis problem," in *Proc. Popov Soc. Meeting*, May 1985, pp. 1–4.
- [91] G. D'Elia, G. Leone, and R. Pierri, "A numerical method in power synthesis of aperture antennas," in *Proc. Int. Symp. Antennas Propag. Soc.*, vol. 24, Jun. 1986, pp. 663–666.
- [92] G. Franceschetti, G. Mazzarella, and G. Panariello, "Array synthesis with excitation constraints," *IEE Proc. H-Microw., Antennas Propag.*, vol. 135, no. 6, pp. 400–407, Dec. 1988.
- [93] O. M. Bucci, G. D'Elia, and G. Leone, "Reflector antenna power pattern synthesis: A general and efficient approach," *IEEE Trans. Antennas Propag.*, vol. 37, no. 7, pp. 875–883, Jul. 1989.
- [94] O. M. Bucci, G. Mazzarella, and G. Panariello, "Reconfigurable arrays by phase-only control," *IEEE Trans. Antennas Propag.*, vol. 39, no. 7, pp. 919–925, Jul. 1991.
- [95] J. A. Encinar, R. Florencio, M. Arrebola, M. A. Salas-Natera, M. Barba, J. E. Page, R. R. Boix, and G. Toso, "Dual-polarization reflectarray in Ku-band based on two layers of dipole arrays for a transmit-receive satellite antenna with South American coverage," *Int. J. Microw. Wireless Technol.*, vol. 10, no. 2, pp. 149–159, 2018.
- [96] C. Tienda, J. A. Encinar, M. Barba, and M. Arrebola, "Dual-polarization Ku-band compact spaceborne antenna based on dual-reflectarray optics," *Sensors*, vol. 18, no. 4, pp. 1–12, Apr. 2018.
- [97] D. R. Prado, A. Campa, M. Arrebola, M. R. Pino, J. A. Encinar, and F. Las-Heras, "Design, manufacture and measurement of a low-cost reflectarray for global Earth coverage," *IEEE Antennas Wireless Propag. Lett.*, vol. 15, pp. 1418–1421, 2016.
- [98] W. P. M. N. Keizer, "Fast low-sidelobe synthesis for large planar array antennas utilizing successive fast Fourier transforms of the array factor," *IEEE Trans. Antennas Propag.*, vol. 55, no. 3, pp. 715–722, Mar. 2007.
- [99] W. P. M. N. Keizer, "Low sidelobe phased array pattern synthesis with compensation for errors due to quantized tapering," *IEEE Trans. Antennas Propag.*, vol. 59, no. 12, pp. 4520–4524, Dec. 2011.
- [100] W. P. M. N. Keizer, "Synthesis of monopulse antenna patterns for elliptical phased array antennas with different peak sidelobes along the principal planes," *IEEE Trans. Antennas Propag.*, vol. 67, no. 9, pp. 5943–5950, Sep. 2019.
- [101] W. P. M. N. Keizer, "Amplitude-only low sidelobe synthesis for large thinned circular array antennas," *IEEE Trans. Antennas Propag.*, vol. 60, no. 2, pp. 1157–1161, Feb. 2012.
- [102] W. P. M. N. Keizer, "Element failure correction for a large monopulse phased array antenna with active amplitude weighting," *IEEE Trans. Antennas Propag.*, vol. 55, no. 8, pp. 2211–2218, Aug. 2007.
- [103] W. P. M. N. Keizer, "Linear array thinning using iterative FFT techniques," *IEEE Trans. Antennas Propag.*, vol. 56, no. 8, pp. 2757–2760, Aug. 2008.
- [104] W. P. M. N. Keizer, "Large planar array thinning using iterative FFT techniques," *IEEE Trans. Antennas Propag.*, vol. 57, no. 10, pp. 3359–3362, Oct. 2009.
- [105] W. P. M. N. Keizer, "Synthesis of thinned planar circular and square arrays using density tapering," *IEEE Trans. Antennas Propag.*, vol. 62, no. 4, pp. 1555–1563, Apr. 2014.

- [106] J. L. A. Quijano and G. Vecchi, "Sparse array synthesis via alternating projections," in *Proc. IEEE Antennas Propag. Soc. Int. Symp.*, Jun. 2009, pp. 1–4.
- [107] J. L. Araque Quijano, G. Vecchi, and M. Sabbadini, "Sparse array synthesis via alternating projections and iterative field synthesis orthogonalization," in *Proc. 5th Eur. Conf. Antennas Propag. (EuCAP)*, Rome, Italy, Apr. 11–15, 2011, pp. 3950–3952.
- [108] D. Pinchera and M. D. Migliore, "Effective sparse array synthesis using a generalized alternate projection algorithm," in *Proc. IEEE Conf. Antenna Meas. Appl. (CAMA)*, Nov. 2014, pp. 1–2.
- [109] D. Pinchera, M. D. Migliore, F. Schettino, M. Lucido, and G. Panariello, "A sparse forcing conformal array synthesis method," in *Proc. IEEE Int. Symp. Antennas Propag. USNC/URSI Nat. Radio Sci. Meeting*, Jul. 2017, pp. 2019–2020.
- [110] F. Veneri, S. Costanzo, G. D. Massa, and G. Angiulli, "An improved synthesis algorithm for reflectarrays design," *IEEE Antennas Wireless Propag. Lett.*, vol. 4, pp. 258–261, 2005.
- [111] D. Trincia, L. Mareaccioli, R. V. Gatti, and R. Sorrentino, "Modified projection method for array pattern synthesis," in *Proc. 34th Eur. Microw. Conf.*, vol. 3. Amsterdam, The Netherlands, Oct. 2004, pp. 1397–1400.
- [112] J. Leonardo, A. Quijano, and G. Vecchi, "Alternating adaptive projections in antenna synthesis," *IEEE Trans. Antenna Propag.*, vol. 58, no. 3, pp. 727–737, Mar. 2010.
- [113] O. M. Bucci, G. D'Elia, and G. Romito, "Power synthesis of conformal arrays by a generalised projection method," *IEEE Proc. Microw. Antennas Propag.*, vol. 142, no. 6, pp. 467–471, Dec. 1995.
- [114] O. M. Bucci and G. D'Elia, "Power synthesis of reconfigurable conformal arrays with phase-only control," *IET Microw., Antennas Propag.*, vol. 145, no. 1, pp. 131–136, Feb. 1998.
- [115] O. M. Bucci, A. Capozzoli, G. D'Elia, and S. Musto, "A new approach to the power pattern synthesis of reflectarrays," in *Proc. URSI Int. Symp. Electromagn. Theory (EMTS)*. Pisa, Italy, May 2004, pp. 1053–1055.
- [116] O. M. Bucci, A. Capozzoli, G. D'Elia, and S. Russo, "Power pattern synthesis of reflectarrays: Comparison between two approaches," in *Proc. 15th Riunione Nazionale di Elettromagnetismo (CD-ROM)*. Cagliari, Italy, Sep. 2004, pp. 1–4.
- [117] O. M. Bucci, A. Capozzoli, G. D'Elia, and S. Russo, "An advanced technique for reflectarray power pattern synthesis and its experimental validation," in *Proc. Int. Symp. Antennas Propag. (ISAP)*. Seoul South Korea, Aug. 2005, pp. 561–564.
- [118] D. R. Prado, A. F. Vaquero, M. Arrebola, M. R. Pino, and F. Las-Heras, "Acceleration of gradient-based algorithms for array antenna synthesis with far-field or near-field constraints," *IEEE Trans. Antennas Propag.*, vol. 66, no. 10, pp. 5239–5248, Oct. 2018.
- [119] D. R. Prado, J. A. Lopez-Fernandez, M. Arrebola, and G. Goussetis, "Support vector regression to accelerate design and crosspolar optimization of shaped-beam reflectarray antennas for space applications," *IEEE Trans. Antennas Propag.*, vol. 67, no. 3, pp. 1659–1668, Mar. 2019.
- [120] D. R. Prado, J. A. López-Fernández, and M. Arrebola, "Efficient general reflectarray design and direct layout optimization with a simple and accurate database using multilinear interpolation," *Electronics*, vol. 11, no. 2, pp. 1–19, Jan. 2022.
- [121] D. R. Prado and M. Arrebola, "Effective XPD and XPI optimization in reflectarrays for satellite missions," *IEEE Antennas Wireless Propag. Lett.*, vol. 17, no. 10, pp. 1856–1860, Oct. 2018.
- [122] M. Ettore, M. Casaletti, G. Valerio, R. Sauleau, L. L. Coq, S. C. Pavone, and M. Albani, "On the near-field shaping and focusing capability of a radial line slot array," *IEEE Trans. Antennas Propag.*, vol. 62, no. 4, pp. 1991–1999, Apr. 2014.
- [123] I. Iliopoulos, M. Casaletti, R. Sauleau, P. Pouliguen, P. Potier, and M. Ettore, "3-D shaping of a focused aperture in the near field," *IEEE Trans. Antennas Propag.*, vol. 64, no. 12, pp. 5262–5271, Dec. 2016.
- [124] I. Iliopoulos, M. Teniou, M. Casaletti, P. Potier, P. Pouliguen, R. Sauleau, and M. Ettore, "Near-field multibeam generation by tensorial metasurfaces," *IEEE Trans. Antennas Propag.*, vol. 67, no. 9, pp. 6068–6075, Sep. 2019.
- [125] G. Xu, R. Zeng, S. Chen, M. Shi, and C. Yu, "A novel synthesis method for millimeter-wave antenna with contoured-beam at near-field region," in *Proc. 47th Eur. Microw. Conf. (EuMC)*, Oct. 2017, pp. 264–267.
- [126] B. Hao, P. Huo, and Z. Li, "Field emulator for wireless communication devices base on programmable metasurface," in *Proc. 14th Eur. Conf. Antennas Propag. (EuCAP)*, Mar. 2020, pp. 1–4.
- [127] A. F. Vaquero, D. R. Prado, M. Arrebola, M. R. Pino, and F. Las-Heras, "Near field synthesis of reflectarrays using intersection approach," in *Proc. 11th Eur. Conf. Antennas Propag. (EuCAP)*, Mar. 2017, pp. 3644–3648.
- [128] A. F. Vaquero, D. R. Prado, M. Arrebola, and M. R. Pino, "Reflectarray antennas for 5-G indoor coverage," in *Proc. 13th Eur. Conf. Antennas Propag. (EuCAP)*. Krakow, Poland, Apr. 2019, pp. 1–4.
- [129] O. M. Bucci, A. Capozzoli, and G. D'Elia, "Power pattern synthesis of reconfigurable conformal arrays with near-field constraints," *IEEE Trans. Antennas Propag.*, vol. 52, no. 1, pp. 132–141, Jan. 2004.
- [130] E. Martinez-de-Rioja, D. Martinez-de-Rioja, J. A. Encinar, A. Pino, B. Gonzalez-Valdes, Y. Rodriguez-Vaqueiro, M. Arias, and G. Toso, "Advanced multibeam antenna configurations based on reflectarrays: Providing multispot coverage with a smaller number of apertures for satellite communications in the k and ka bands," *IEEE Antennas Propag. Mag.*, vol. 61, no. 5, pp. 77–86, Oct. 2019.
- [131] M. Zhou, S. B. Sorensen, Y. Brand, and G. Toso, "Doubly curved reflectarray for dual-band multiple spot beam communication satellites," *IEEE Trans. Antennas Propag.*, vol. 68, no. 3, pp. 2087–2096, Mar. 2020.
- [132] S. Liu, L. Xiao, M. Zhao, X. Xu, and Y. Li, "Performance analysis of intelligent reflecting surface in multi-user MIMO systems," in *Proc. 5th Annu. Int. Conf. Inf. Syst. Artif. Intell. (ISAI)*. Zhejiang, China, May 2020, pp. 1–10.



**DANIEL R. PRADO** was born in Sama de Langreo, Asturias, Spain, in 1986. He received the B.Sc., M.Sc., and Ph.D. degrees in telecommunication engineering from the University of Oviedo, Gijón, Spain, in 2011, 2012, and 2016, respectively.

From 2010 to 2011, he was with the Institute of Electronics, Communications and Information Technology, Queen's University Belfast, Belfast, U.K., where he was involved in the design of leaky-wave antennas as a part of his B.Sc. research project. From 2011 to 2017, he was a Research Assistant with the Signal Theory and Communications Area, University of Oviedo, where he was involved in the development of efficient techniques for the analysis and synthesis of reflectarray antennas. In 2014, he was with the School of Electrical Engineering, KTH Royal Institute of Technology, Stockholm, Sweden, as a Visiting Scholar, where he was involved in transformation optics applied to dielectric lenses. From 2018 to 2019, he was with the Institute of Sensors, Signals and Systems, Heriot-Watt University, Edinburgh, U.K. Since 2020, he has been with the Signal Theory and Communications Area, University of Oviedo, as a Postdoctoral Researcher. His current research interests include the analysis of uniform and nonuniform arrays, and the development of efficient techniques for the analysis and optimization of near and far fields of spatially-fed antennas, including reflectarrays and transmitarrays.

Dr. Prado was a recipient of a Predoctoral Scholarship financed by the Gobierno del Principado de Asturias, a Postdoctoral Fellowship partially financed by the European Union, and a Postdoctoral Fellowship financed by the Spanish Government.

• • •